ChemPubSoc Europe

DOI: 10.1002/ejoc.201901164

EurJOC European Journal of Organic Chemistry

Full Paper

Enantioselective Recognition

Synthesis of Isotopically Labelled Disparlure Enantiomers and Application to the Study of Enantiomer Discrimination in Gypsy Moth Pheromone-Binding Proteins

Govardhana R. Pinnelli,[a] Mailyn Terrado,[a] N. Kirk Hillier,[b] David R. Lance,[c] and Erika Plettner*[a]

Abstract: To study the binding mechanism of disparlure (7,8)-epoxy-2-methyloctadecane enantiomers with pheromone-binding proteins (PBPs) of the gypsy moth, oxygen-17 or 18 and 5,5,6,6-deuterium labelled disparlure enantiomers were prepared in an efficient, enantioselective route. Key steps involve the asymmetric α-chlorination of dodecanal by SOMO catalysis and Mitsunobu inversion of a 1,2-chlorohydrin. The pheromone, (+)-disparlure (7*R*, 8*S*), was tested in two infested zones, demonstrating that it is very attractive towards male gypsy moths. Studies of the binding of (+)-disparlure and its antipode to gypsy moth PBPs by ^{2}H &^{17}O NMR at 600 MHz are reported. Chemical shifts, spin-lattice relaxation decay times (T_1) and transverse relaxation decay times (T_2) of deuterium atoms of disparlure enantiomers in ^{2}H NMR show that the binding of disparlure enantiomers to PBP1 differs from binding to PBP2, as expected from their opposite binding preferences (PBP1 binds (–)-disparlure, and PBP2 binds (+)-disparlure more strongly). Models of the disparlure enantiomers bound to one internal binding site and two external binding sites of both PBPs were constructed. The observed chemical shift changes of deuterated ligand signals, from non-bound to bound, T_1 and T_2 values are correlated with results from the simulations. Together these results suggest that the disparlure enantiomers adopt distinct conformations within the binding sites of the two PBPs and interact with residues that line the sites.

Introduction

The gypsy moth, *Lymantria dispar*, is a harmful pest of a large variety of trees (oak, apple, maple, mountain ash, pine, and spruce), causing serious forest losses during outbreaks in Europe, Asia and North America. (+)-Disparlure (+)-**1** (Figure 1), (7*R*, 8*S*)-epoxy-2-methyloctadecane is the sex attractant pheromone, produced and released by female gypsy moths and detected by the male moths. Initially, disparlure was identified as *cis*-(7, 8)-epoxy-2-methyloctadecane by Bierl and co-workers in 1970.[1] Later, Iwaki et al. demonstrated the absolute stereochemistry of disparlure by synthesizing both enantiomers, testing them in the field, and reporting that (+)-disparlure (+)-**1** is more active than (–)-disparlure (–)-**1** (Figure 1).[2] It has been shown that the highest number of moths can be caught in traps when the most enantiopure (+)-disparlure (> 99 % ee) is used.[2] Studies have shown that the disparlure enantiomers bind strongly to pheromone binding proteins 1 and 2 (PBP1 & PBP2), with opposite enantioselectivity.[3,4] However, the binding mechanism of pheromone with PBPs offers some unanswered questions. Our group proposed previously a two-step association mechanism, based on kinetic studies with ligand and PBPs. The kinetic data suggested that a ligand will interact with the protein on an external site before entering the internal

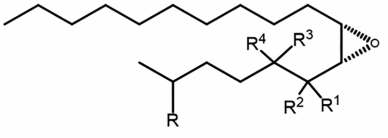

(+)-**1** : R = CH_3 ; R^1, R^2, R^3 & R^4 = H : (+)-**disparlure**

(+)-**1a** : R = H ; R^1, R^2, R^3 & R^4 = H : (+)-**monachalure**

(+)-**1b** or (+)-**1c** : R = CH_3 ; O = $^{17/18}O$; R^1, R^2, R^3 & R^4 = D : $^{17/18}$**O &** ^{2}**H (+)-disparlure**

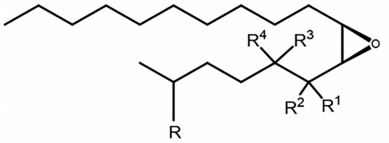

(-)-**1** : R = CH_3 ; R^1, R^2, R^3 & R^4 = H : (-)-**disparlure**

(-)-**1b** or (-)-**1c**: R = CH_3 ; O = $^{17/18}O$; R^1, R^2, R^3 & R^4 = D : $^{17/18}$**O &** ^{2}**H (-)-disparlure**

Figure 1. Structures of disparlure enantiomers and (+)-monachalure, prepared during optimization of the (+)-disparlure synthesis.

[a] *Dept. of Chemistry, Simon Fraser University, 8888 University Dr., Burnaby B. C. V5A 1S6, Canada*
E-mail: plettner@sfu.ca
[b] *Dept. of Biology, Acadia University, 33 Westwood Ave., Wolfville, NS B4P 2R6, Canada*
[c] *USDA-APHIS-PPQ CPHST Otis Laboratory, 1398 W Truck Rd, Buzzards Bay, MA 02542, USA*

Supporting information and ORCID(s) from the author(s) for this article are available on the WWW under https://doi.org/10.1002/ejoc.201901164.

binding pocket.[3] Once the ligand reaches the internal pocket we know that the two gypsy moth PBPs differ in their affinity for the disparlure enantiomers, but there only are *in-silico* docking models of the PBP-bound pheromones.[5,6] The challenge of binding studies of PBP-ligand interactions using already known assays is to probe the equilibrating PBP-ligand mixture without excessively disturbing it and to detect the bound ligand. Therefore, we aimed to prepare ^{17}O or ^{18}O & ^{2}H labelled (+)-disparlure (+)-**1b** or (+)-**1c** and (–)-disparlure (–)-**1b** or (–)-**1c** (Figure 1) and study their binding orientation with pheromone binding proteins using ^{17}O and ^{2}H NMR spectroscopy. We correlated results from ^{2}H NMR experiments with *in-silico* docking models at one internal and two external binding sites of PBP1 and PBP2.

To date, more than twenty synthetic routes to synthesize (+)-disparlure have been reported.[7] These methods are based on either asymmetric synthesis or chiral pool precursors. Most of the synthetic routes have utilized Sharpless asymmetric epoxidation[8] and dihydroxylation,[9,7d,7e] whereas other synthetic routes used chiral stannanes,[10] enantiopure sulfoxides,[11] asymmetric chloroallylboration,[12a] asymmetric MacMillan's self-aldol reaction[12b] and chiral pool starting materials such as L-glutamic acid,[13] L-tartaric acid[14] and D-glucose-δ-lactone.[7m] The drawbacks of previously reported approaches include the use of uncommon starting materials, low enantiomeric excess of the final (+)-disparlure, many steps and low overall yield. For example, disparlure currently used for monitoring programs in the field is prepared by Sharpless epoxidation of (*Z*)-tridec-2-en-1-ol, to access the chiral epoxide ring, and Wittig olefination of the epoxy aldehyde to install the branched alkyl side chain. Typically, the overall yield of this route is 33 % from non-commercially available starting material and enantiomeric excess values range from 91–95 %.[8b] Here we describe a route to (+)-disparlure that is one step shorter (counting from commercial starting material), has an overall yield in the range of 42–53 % and an enantiomeric excess of > 99 %. Apart from that, this route provides easy access to isotope (^{17}O, ^{18}O and ^{2}H) labelled disparlure enantiomers for studies with pheromone binding proteins (PBPs) and degrading enzymes that are present in the male gypsy moth antennae.

Disparlure Enantiomer and PBP Interaction

The remarkable enantiomer discrimination between (+)-disparlure and (–)-disparlure is governed by the selectivity and sensitivity of neurons of the olfactory receptors, which are located in the sensory hairs of male moth antennae.[3,4,15] Sensory hairs are hollow, and the interior space of the hairs is filled with sensillar lymph, which contains the abundant, soluble PBPs.[16] The sensory hairs also house the dendrites of 2–3 chemosensory neurons, which are responsible for detecting any odorants that enter the lymph via pores on the sensillar cuticle.[17] The PBPs are believed to control the diffusion of pheromones and other odors to olfactory neurons in the dendritic membrane. The gypsy moth has two known PBPs: *Ldis*PBP1 and *Ldis*PBP2, and these proteins are known to have opposite affinities for (+)- and (–)-disparlure.[18,19] Furthermore, the two proteins differ in their ligand binding and dissociation kinetics: PBP2 binds ligands at its internal binding site very slowly,[4] whereas PBP1 has much faster association and dissociation kinetics. The interaction and discrimination of these two PBPs towards disparlure enantiomers are not completely understood due to lack of crystal or NMR-based structures.

Here we describe a short synthesis of enantiopure, labelled and non-labelled disparlure, followed by experiments in which we studied the kinetics of non-labelled disparlure enantiomer association and dissociation with PBP1, the binding of ^{17}O-disparlure to PBP1 and of ^{18}O/5,5,6,6-deuterium labelled disparlure enantiomers to both PBPs. With the latter, two types of analysis were done on the data: 1) chemical shift changes between disparlure in buffer vs. bound to PBP were correlated with the location of the deuterium labels in PBP-ligand structures obtained through docking simulations, and 2) the measurement of longitudinal relaxation (T_1) and transverse relaxation (T_2) times. Docking simulations of both enantiomers were done with homology models of *L. dispar* PBP1 and PBP2, at one internal and two external binding sites. These were used to interpret the position of disparlure ligands relative to aromatic residues in the protein and the level of mobility of the labeled positions of disparlure under various conditions (in organic solvent, in buffer and bound to the PBPs). We then correlated the simulations with the observed NMR parameters. We detected differences between the enantiomers of disparlure interacting with the two proteins. This is discussed in the context of differences detected in other assays.

Results and Discussion

Synthesis

Herein we report an efficient total synthesis of (+)-disparlure, (–)-disparlure, isotope labelled disparlure enantiomers and (+)-monachalure (7*R*, 8*S*)-epoxyoctadecane, the pheromone of the nun moth, *Lymantria monacha* (Figure 1), in five steps. This work has resulted in preparation of optically pure (+)-disparlure in large quantities (>1 g). The (+)-disparlure was tested in two infested zones, demonstrating that it is very attractive towards male gypsy moths (see below).

We explored the use of MacMillan's procedure of SOMO-activated α-chlorination of an aldehyde to prepare enantiopure α-chloroaldehyde[20,21] Chlorination of dodecanal **2** by LiCl as the chlorine source, in the presence of an imidazolidinone catalyst afforded the enantiopure α-chlorododecanal (+)-**3** (Scheme 1) in 87 % yield. The enantiopurity of α-chlorododecanal was determined to be >99 % by chiral HPLC (see Supplementary Information).

With the highly enantiopure α-chloroaldehyde in hand, we next turned our attention to the diastereoselective addition of organometallic reagents.[22–25] For the optimization of this step we used the non-branched building block that results in (+)-monachalure (+)-**1a** (Scheme 1). The addition of either *n*-hexyllithium or Grignard reagent (hexylmagnesium bromide) to α-chloroaldehyde (+)-**3** afforded chlorohydrins in good yield but in moderate diastereomeric excess (Table 1, entries 3 & 4).

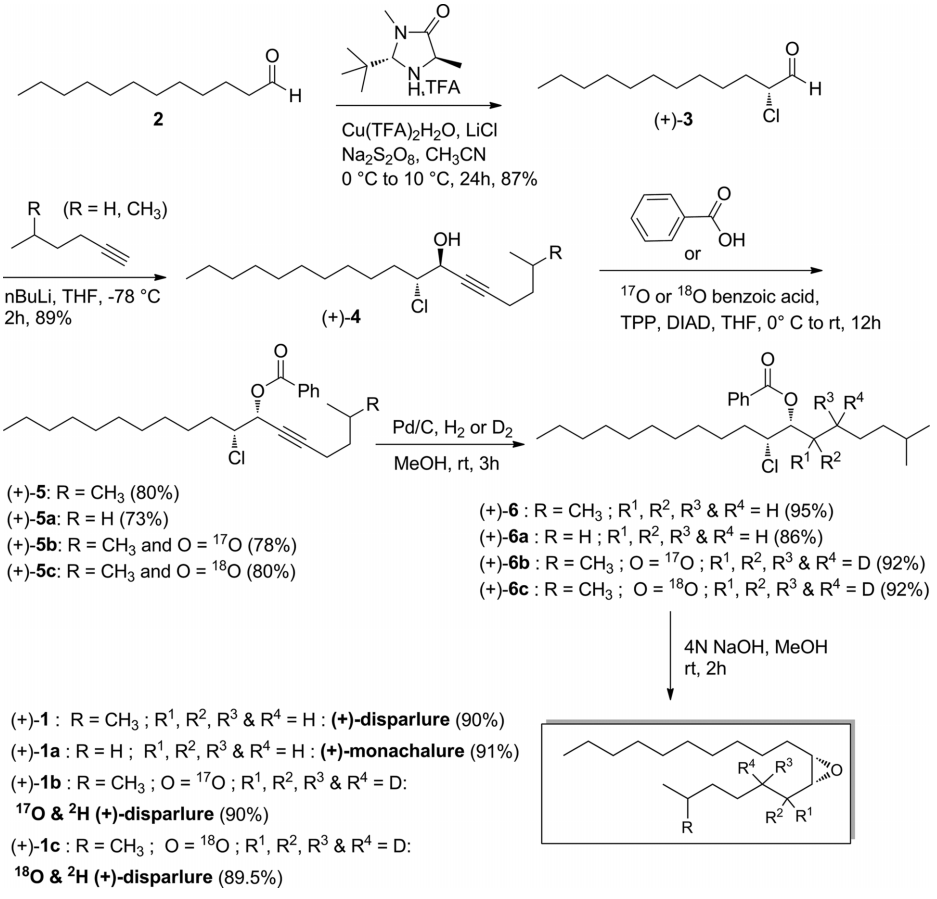

Scheme 1. The synthetic route to (+)-monachalure, to non-labelled and isotope labelled (+)-disparlure developed here.

A brief survey of solvents (Et_2O, THP) failed to significantly improve diastereoselectivity of carbon nucleophile addition. Finally, we treated α-chloroaldehyde (+)-**3** with the alkyne lithium anion derived from 1-hexyne or 5-methyl 1-hexyne: the reaction proceeded cleanly and the product 1,2-*anti*-chlorohydrin (+)-**4** was isolated in good yield with a 20:1 diastereoselectivity. At this point, the diastereomers were separated by flash column chromatography.

Table 1. Addition of organometallic reagents to enantiopure α-chloroaldehyde (+)-**3**.

Entry	Solvent	Compound	Organometallic reagent	Diastereoselectivity[a]
1	THF	(+)-**3**	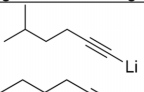	20 : 1
2	THF	(+)-**3**	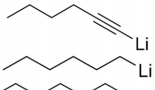	20 : 1
3	THF	(+)-**3**		10 : 1
4	THF	(+)-**3**	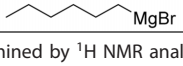	3 : 1

[a] Ratio of diastereomers determined by ^{1}H NMR analysis of crude product.

If the 1,2-*anti* chlorohydrin (+)-**4** (Scheme 1) is treated with base, then a *trans* epoxide is formed. However, we require a 1,2-*syn* product to obtain the *cis* epoxide. Therefore, we need to invert the stereochemistry either at the C-8 or C-9 position of the 1,2-*anti*-chlorohydrin (+)-**4**. An attempt was made to invert the stereochemistry at the C-9 position by a Finkelstein reaction, but the reaction was unsuccessful, and the starting material was recovered.

In order to prepare 1,2-*syn* product, the stereochemistry at the C-8 carbon of compound (+)-**4** was inverted by a Mitsunobu reaction. We treated compound (+)-**4** with TPP (triphenylphosphane) DIAD (diisopropyl azadicarboxylate) and benzoic acid in dry THF under an inert atmosphere. This afforded complete inversion product (+)-**5**, which was isolated in 80 % yield. Hydrogenation of compound (+)-**5** with H_2 and catalytic Pd/C in methanol afforded reduced product in 95 % yield, which was treated with 4 N NaOH solution in methanol, to produce the final product (+)-disparlure (+)-**1** in 90 % yield. The spectroscopic data (^{1}H NMR, ^{13}C NMR, IR, $[\alpha]_D$ and MS) of (+)-**1** are identical to those reported in the literature.[2,7b]

For the synthesis of (–)-disparlure (Scheme S1, Supporting Information), D-SOMO (2*R*, 5*S*)-2-(*tert*-butyl)-3,5-dimethylimidazolidin-4-one) was used to prepare enantiopure α-chlorododecanal (–)-**3**. Diastereoselective addition of (–)-**3** with lithium alkyne anion resulted in (–)-**4** in 85 % yield. Reaction of (–)-**4** with benzoic acid and DIAD produced the ester, which was hydrogenated with H_2 and Pd/C, then treated with NaOH to close the epoxide and furnish (–)-disparlure (–)-**1** in 90 % yield.

Synthesis of ^{17}O or ^{18}O enriched compounds usually involves water, carbon monoxide and [$^{17/18}$O] enriched starting materials,[26,27] which are expensive. The most convenient precursor

to prepare $^{17/18}O$ enriched compounds is labelled water, which is commercially available with various enrichment levels starting from 10 to 97 %. To prepare isotope labelled disparlure enantiomers, we obtained ^{17}O or ^{18}O labelled benzoic acid by hydrolysis of benzoyl chloride with ^{17}O or ^{18}O water (20 atom-% ^{17}O or 97 atom-% ^{18}O). Further, the ^{17}O or ^{18}O labelled intermediates (+)-**5b**, (+)-**5c**, (–)-**5b** and (–)-**5c** (Scheme 1) were prepared by Mitsunobu reaction of intermediates (+)-**4** and (–)-**4** with ^{17}O or ^{18}O labelled benzoic acid. The labelled intermediates were obtained as liquids, which contained approximately 50 % ^{18}O and 15–20 % ^{17}O at either one of the benzoate oxygens. Through the subsequent deuteration of (+)-**5b**, (+)-**5c**, (–)-**5b** and (–)-**5c** with D_2 in the presence of Wilkinson's catalyst, the products (+)-**6b**, (+)-**6c**, (–)-**6b** and (–)-**6c** were obtained. Finally, the target compounds (+)-**1b**, (+)-**1c**, (–)-**1b** and (–)-**1c** were obtained by basic epoxide ring closure of (+)-**6b**, (+)-**6c**, (–)-**6b** and (–)-**6c** with NaOH. The percentages of ^{17}O or ^{18}O at the epoxide oxygen of the target compounds were calculated from the area of the shifted carbon signal in their ^{13}C NMR spectra and from HR-MS (Figure 2 and Table 2). The ^{17}O NMR spectrum was obtained for the ^{17}O labelled (+)-disparlure (Figure 2d). In ^{18}O labelled (+)-disparlure, the signals for the oxirane ring carbon atoms were seen upfield from those of the non-labelled variant due to the isotope effect on the chemical shift.

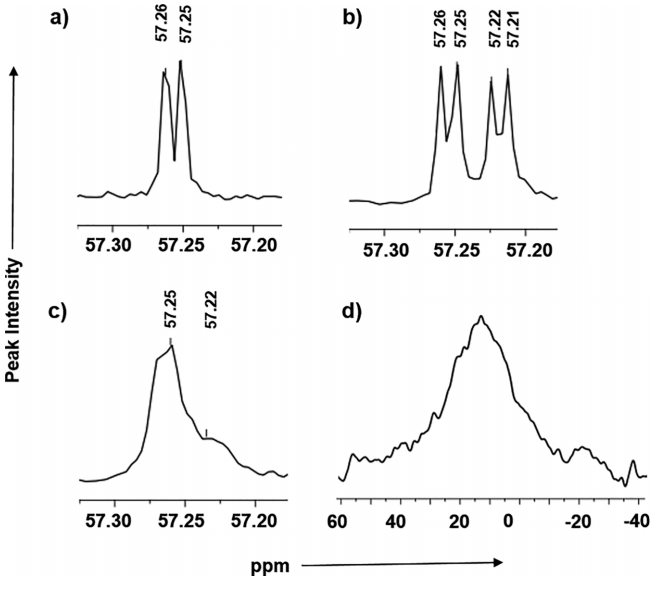

Figure 2. ^{13}C NMR signals of epoxy carbons of a) (+)-disparlure, b) ^{18}O (+)-disparlure c) ^{17}O (+)-disparlure, and d) ^{17}O NMR spectrum of ^{17}O (+)-disparlure in $CDCl_3$.

Table 2. Oxygen and hydrogen isotope enrichment of (+)-and (–)-disparlure.

Entry	Compound	Isotope enrichment [%] ^{17}O	^{18}O	^{2}H (C-5 & 6)
1	(+)-**1b**	8–10		> 99
2	(+)-**1c**		50	> 99
3	(–)-**1b**	8–10		> 99
4	(–)-**1c**		50	> 99

Determination of Enantiopurity

The common method for finding enantiopurity of chiral organic molecules is the conversion of enantiomers to diastereomers by introducing a second defined chiral center.[28] To optimize the method used to determine enantiomeric excess of (+)-disparlure, we converted a scalemic sample of disparlure **7** (Supporting Information, Scheme S3) to the corresponding *cis*-N-(α-methylbenzyl)aziridines with inversion of configuration at both, the 7 and 8 positions.[29] The *cis* epoxide of scalemic disparlure was opened with *R*-(+)-α-methylbenzylamine in the presence of trimethylaluminium, which produced a mixture of amino alcohols. The amino alcohols were treated with methanesulfonyl chloride and triethylamine, to afford a diastereomeric mixture of *cis*-N-(α-methylbenzyl) aziridines **16** and **17**. Then the diastereomeric aziridines were resolved by gas chromatography, and we observed nearly baseline separation of the peaks. The diastereomers of *cis*-N-(α-methylbenzyl)aziridine **16** and **17** were observed at 53.05 and 53.40 min, respectively. Similarly, (+) and (–)-disparlure (+)-**1** and (–)-**1** were converted to corresponding *cis*-N-(α-methylbenzyl)aziridine and found to be in enantiomeric excess (> 99 %) (see Supporting Information, Scheme S4 and Scheme S5, Figure S2).

Field Test of (+)-1

(+)-Disparlure (+)-**1** prepared herein was tested in two infested zones, located in Massachusetts (USA) and Nova Scotia (Canada), to demonstrate activity against male gypsy moths. We used delta sticky traps baited with either white rubber septa (Nova Scotia) or milk carton traps baited with impregnated dental cotton (Massachusetts), in both cases dosed with 500 µg of (+)-disparlure or 500 µg of paraffin oil in hexanes as a control. In Massachusetts, milk carton traps with cotton wick dispensers were used and left for 4 days. Three different doses (100, 500 and 1000 µg) were tested against a control with mineral oil. The 100 and 1000 µg treatments were from a commercial standard, and the 500 µg dose was from this study. The control did

Table 3. Summary of field trails.

Location	Trap type	Dispenser	Treatment	Dose [µg]	Moths caught (mean ± SEM, n = 10)
Massachusetts	Milk carton	Cotton wick	Control (mineral oil)	500	0 ± 0
			(+)-disparlure commercial standard	100	52 ± 15
			(+)-disparlure (this study)	500	70 ± 8
			(+)-disparlure commercial standard	1000	82 ± 17
Nova Scotia	Delta	Rubber septum	Control (mineral oil)	500	0.9 ± 0.4
			(+)-disparlure (this study)	500	22 ± 2

not catch any moths, and the pheromone-baited traps caught the same number of moths within limits of error (F = 2.27; *d.f.* = 2, 8; P = 0.17) (Table 3). Significant contamination with (–)-disparlure (due to insufficiently high ee) on a 500 µg wick would normally suppress trap catch to levels significantly below those obtained with highly pure (+)-disparlure at either 100 µg or 1000 µg loadings.[41] In Nova Scotia, red delta traps with rubber septum dispensers were used and left for 10 days. Three of the treatment traps were lost due to predation. Nonetheless, the treatment traps caught significantly more moths than the control (Table 3). Observation on the first day suggested that traps saturated with moths within a matter of hours. The traps attracted moths within minutes of being deployed. Traps in the two locations caught different total numbers of moths due to two factors: 1) different infestation levels and 2) different dispensers and traps.

Heteronuclear NMR Studies of Disparlure Binding to PBPs

The binding of disparlure enantiomers to pheromone binding proteins of male gypsy moth was studied by NMR spectroscopy. First, we studied binding of ^{17}O disparlure to *Ldis*PBP1, as well as ^{17}O disparlure by itself in $CDCl_3$ (Figure 2d) and in buffer. The ^{17}O signal was broad, as expected, in $CDCl_3$, but completely disappeared when disparlure was placed in buffer with fatty acid salts as emulsifier and a bridging solvent (acetonitrile). We chose to use fatty acid micelles to disperse disparlure in the aqueous buffer, because previous studies from our laboratory have shown that gypsy moth sensilla contain high quantities of fatty acids in the lymph.[30] The result suggests that disparlure mobility would have decreased significantly in the fatty acid micelles and, therefore, the ^{17}O signal is so broad that it cannot be detected.

Because ^{17}O was difficult to detect, we decided to use ^{2}H labelled disparlure enantiomers (+)-**1c** and (–)-**1c** (Scheme 1 and Scheme S1) in our binding studies. We used 600 MHz deuterium NMR to observe binding-induced chemical shift change of the deuterium signals of the deuterated disparlure enantiomers. The ^{2}H chemical shift of the deuterium labelled disparlure enantiomers (+)-**1c** or (–)-**1c** resonance in the presence and absence of *Ldis*PBPs was monitored. It was possible to distinguish the more shielded 5-D signals from the 6-D signals (Figure 3). We have named these signals 5-D_a, 5-D_b, 6-D_a and 6-D_b. In a solvent ($CDCl_3$, toluene or phosphate buffer) the majority of disparlure molecules will adopt a conformation around the epoxide at or near the global energy minimum.[5] In that conformation, (+)-**1c** has the 5-*pro*-R H atom in the shielding zone above the epoxide ring and the 5-*pro*-S H atom in the deshielding zone at the edge of the epoxide ring, along the C-O bond.[31] In our data, 5-D_a is more shielded than 5-D_b (Table 4),

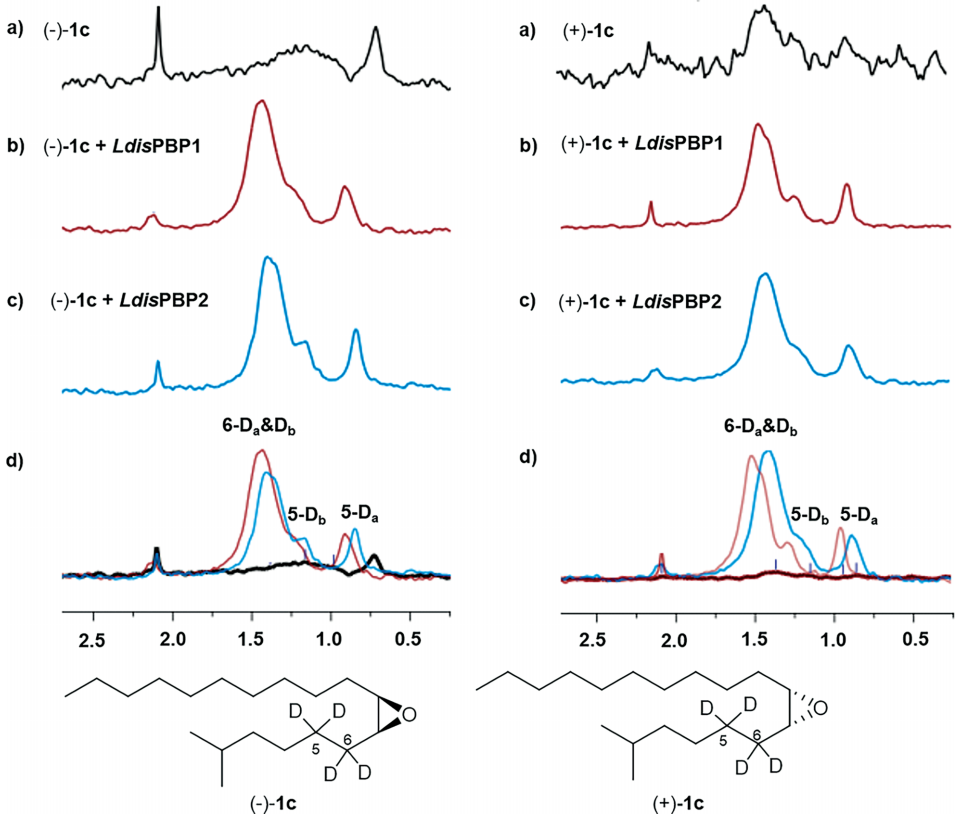

Figure 3. The 600 MHz ^{2}H NMR spectra recorded for deuterium labelled disparlure enantiomers with and without *Ldis*PBPs in phosphate buffer at pH 8. The chemical shift scales of the above spectra are aligned on the basis of the deuterium resonance (2.10 ppm) of internal standard CH_3CN. a) The region of the ^{2}H NMR spectra of deuterium labelled disparlure enantiomers and acetonitrile resonances are shown in the absence of *Ldis*PBPs, b) & c) downfield shifting of the deuterium signals of the disparlure enantiomers by *Ldis*PBP1 and *Ldis*PBP2, respectively. d) superimposed spectra of a), b) and c). The same buffer (50 mM sodium phosphate pH 8.0) was used for all these spectra.

Table 4. The ^2H chemical shifts of 5,6-D_4 (+)-**1c** and (–)-**1c** in the presence and absence of *Ldis*PBPs.

Compound	Position signal & assignment[a]		δ $CDCl_3$	δ Toluene	δ Phosphate buffer (pH 8)	δ Phosphate buffer (pH 8) + *Ldis*PBP1[b]	δ Phosphate buffer (pH 8) + *Ldis*PBP2[b]
(+)-**1c**	5-D_a[1]	*pro*-R	0.8	0.94	0.73	0.96 (*pro*-R)	0.89 (*pro*-S)
	5-D_b[1]	*pro*-S	1.07	1.26	0.98	1.30 (*pro*-S)	1.17 (*pro*-R)
	6-D_a[1]	*pro*-S	1.25	1.46	1.16	1.45 (*pro*-S)	1.41 (*pro*-S)
	6-D_b[1]	*pro*-R	1.34	1.56	1.38	1.52 (*pro*-R)	1.45 (*pro*-R)
(–)-**1c**	5-D_a[1]	*pro*-S	0.8	0.94	0.73	0.91 (*pro*-R)	0.85 (*pro*-R)
	5-D_b[1]	*pro*-R	1.07	1.26	0.98	1.21 (*pro*-S)	1.17 (*pro*-S)
	6-D_a[1]	*pro*-R	1.25	1.46	1.16	1.43 (*pro*-R)	1.37 (*pro*-S)
	6-D_b[1]	*pro*-S	1.34	1.56	1.38	1.49 (*pro*-S)	1.41 (*pro*-R)

[a] Assignments of the 5 and 6 deuterium atom signals for disparlure in solvent, based on the global energy minimum around the epoxide found in ab initio calculations in[3] and the anisotropic effect of the oxirane ring.[31] [b] Chemical shifts and assignment, based on averaged protein-bound conformations of the disparlure enantiomers, chemical shift differences between protein-bound and solvent (Table 5) and anisotropic effects of the oxirane and the proteins (see Figure 5).

so 5-D_a must correspond to the *pro*-R D atom and 5-D_b must be the *pro*-S. For (–)-**1c**, the 5-*pro*-S H atom is in the epoxide shielding zone (above the oxirane ring) and the 5-*pro*-R H is in the deshielding zone at the global minimum.[5] Therefore, for this compound, 5-D_a must correspond to the *pro*-S D, whereas 5-D_b must correspond to the *pro*-R D. Using the same approach, we assign the deuterium atoms at the 6 position as 6-D_a = 6-D_S and 6-D_b = 6-D_R for **(+)-1**, and 6-D_a = 6-D_R and 6-D_b = 6-D_S for **(–)-1**. In the chiral protein binding pockets this assignment can change, because there are numerous anisotropic effects (from aromatic side chains and carbonyl groups), apart from the anisotropic effect of the oxirane ring (see below).

The ^2H NMR spectrum of the compounds (+)-**1c** and (–)-**1c** in buffer, in the absence of *Ldis*PBPs showed two peaks, but these were not well resolved due to poor solubility of the compounds in the phosphate buffer solution (Figure 3a). The most shielded 5-D signal was sharper than the 6-D and the second 5-D signals. One explanation is that disparlure forms micelles in the aqueous environment and the mobility of the 6-position is more restricted than that of the 5-position. Furthermore, the hydrophobic disparlure molecule adsorbs on glass surfaces,[30] and the adsorbed molecules will have very restricted mobility and, therefore, broad signals. Addition of *Ldis*PBPs causes an increase in solubility of the (+)-**1c** and (–)-**1c** in the phosphate buffer solution,[3,30] and deuterium resonances to shift downfield (Figure 3b and Figure 3c, Table 4, Table 5 and Table 6). The ^2H chemical shift changes of the bound (+)-**1c** and (–)-**1c** noticed were typically of the order of 0.07 to 0.29 ppm (Table 6). The deuterium signals of (+)-**1c** were more deshielded than signals of (–)-**1c** by *Ldis*PBP1 and *Ldis*PBP2. The apparent bound chemical shift difference of the compounds (+)-**1c** and (–)-**1c** deuterium signals shows that the binding (and therefore local variations in the magnetic field) of disparlure enantiomers to *Ldis*PBP1 is different from binding to *Ldis*PBP2.

Both PBPs have one internal binding site and multiple external binding sites,[5] which interact with a ligand in a stepwise manner, fast external binding, followed by slow internalization.[4] The apparent equilibrium constant for the external sites, K_d', is the ratio of the dissociation and association rate constants, k_{off}/k_{on}, for the first external binding step (Figure 4). From[4] we had data for PBP2, but for PBP1 we lacked data because this protein interacts with ligands much faster than PBP2.[18] Therefore, we used stopped-flow experiments to obtain k_{off} and k_{on} for PBP1 and the disparlure enantiomers from competitive kinetics between a fluorescent reporter ligand (1-phenylnaphthylamine, NPN) and **(+)-1** or **(–)-1**. This information was required to process the *in silico* ligand docking data (see below). For the measurement of association, NPN bound to PBP is displaced with disparlure (which causes NPN fluorescence to decrease). For measurement of disparlure dissociation,

Table 5. Chemical shift differences, relative to the CD_3CN signal, used as an internal standard and net shifts of (+)-**1c** and (–)-**1c** in buffer and PBP-bound.

Condition	δδ (CD_3CN-5-D_a), ppm	δδ (CD_3CN-5-D_b), ppm	δδ (CD_3CN-6-D_a), ppm	δδ (CD_3CN-6-D_b), ppm
$CDCl_3$	1.3	1.03	0.85	0.76
Toluene	1.16	0.84	0.64	0.54
Phosphate buffer	1.37	1.12	0.94	0.72
***Ldis*PBP1 (+)-1c**	1.14	0.85	0.65	0.58
***Ldis*PBP2 (+)-1c**	1.21	0.93	0.69	0.65
***Ldis*PBP1 (–)-1c**	1.19	0.89	0.67	0.61
***Ldis*PBP2 (–)-1c**	1.25	0.93	0.73	0.69

Table 6. Net shifts of (+)-**1c** and (–)-**1c** in buffer and PBP-bound.

Condition	δδ (*Ldis*PBP1-buffer), ppm				δδ (*Ldis*PBP2-buffer), ppm			
	5-D_a	5-D_b	6-D_a	6-D_b	5-D_a	5-D_b	6-D_a	6-D_b
*Ldis*PBP + Buffer + **(+)-1c**	0.23	0.32	0.29	0.14	0.16	0.19	0.25	0.1
*Ldis*PBP + Buffer + **(–)-1c**	0.18	0.2	0.27	0.11	0.12	0.19	0.21	0.07

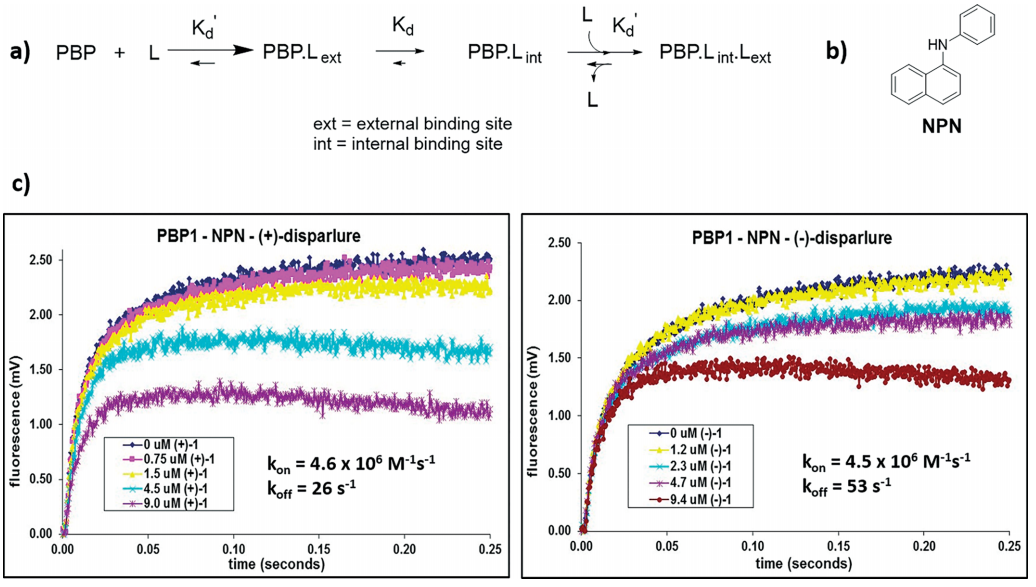

Figure 4. Association and dissociation kinetics of PBPs and cognate ligands. **a)** Kinetic scheme for ligand-PBP interaction. The ligand first binds externally in a rapid, reversible manner, and then slowly diffuses into the internal binding site of the PBP. **b)** Structure of NPN, the competitive fluorescent reporter ligand used in PBP1-ligand association kinetics experiments in a stopped-flow apparatus. **c)** Stopped-flow kinetics with fluorescence reporting of PBP1 with either **(+)-1** or **(–)-1** and NPN. Both association (k_{on}) and dissociation (k_{off}) rate constants can be obtained from non-linear fitting of the traces at different concentrations of ligand and constant concentration of NPN reporter.

Table 7. Dissociation constants used in the calculation of ligand distribution between internally, externally bound and free states. Distributions between states obtained for each PBP with both disparlure enantiomers.

Protein	Ligand	K_d[a] [μM]	K_d'[b] [μM]	Ref. K_d'	% bound internal[c]	% bound external[d]	% free
PBP1	**(+)-1**	6.8	56.5	This work	48.9	43.8	7.3
	(–)-1	6.0	11.8	This work	49.0	49.1	1.9
PBP2	**(+)-1**	2.2	1.1	[4]	49.6	50.2	0.2
	(–)-1	4.7	1.6	[4]	49.2	50.5	0.3

[a] From Terrado et al.[33] [b] Calculated as k_{off}/k_{on}, the ratio of association and dissociation rate constants. [c] $[PBP]_{total}$ = 300 μM; $[L]_{total}$ = 600 μM. [d] Since there are two external binding sites, their combined concentration is 600 μM.

disparlure bound to PBP is displaced with NPN (which causes NPN fluorescence to increase. Both measurements can be done simultaneously in experiments wherein NPN and disparlure compete for the binding sites on the protein (Figure 4).

To understand the chemical shift changes observed, we performed *in-silico* docking simulations of **(+)-1** and **(–)-1** into homology models of PBP1 and PBP2. We docked both ligands into the internal binding site (site 1) and the two largest external sites (sites 2 and 3). The two external sites were assumed to contribute randomly (i.e. equally). Structures that were calculated to be populated > 5 % were examined with regard to the interactions of the focal hydrogen atoms, at the 5 and 6 positions of disparlure, with the protein. Anisotropic effects from aromatic side chains and carbonyl groups within a range of 4.5 Å around the focal H atoms were scored (see experimental section), along with the anisotropic effect from the oxirane ring. Scores were weighted according to their proportion at the docking site, and internal vs. external sites were weighted according to their proportion (Table 7). The patterns obtained for the *pro*-R and *pro*-S hydrogen atoms at each position allowed us to assign signals in the PBP-ligand treatments (Figure 5).

As shown in Figure 5, the assignments for D_a and D_b were reversed in some cases of PBP-bound disparlure enantiomers, relative to those at the global minima. Specifically, for **(–)-1** bound to PBP1,5-D_a is *pro*-R and 5-D_b is *pro*-S. For **(+)-1** bound to PBP2, 5D_a is *pro*-S and 5-D_b is *pro*-R. Finally, for **(–)-1** bound to PBP2,5-D_a = *pro*-R, 5-D_b = *pro*-S, 6-D_a = *pro*-S and 6-D_b = *pro*-R. There are two factors which influence the chemical shifts of the 5 and 6 protons of disparlure when bound to the PBPs: 1) the conformation of the pheromone and 2) the shielding and deshielding effects of nearby groups on the protein, particularly carbonyl or phenyl groups. For example, Figure 6 shows the most populated pose at the internal binding site for the four cases studied here. The disparlure enantiomers are clearly not bound at a minimum conformation calculated in.[5] For the PBP1 and **(–)-1** case, one can see that 5-H_R is in the weak shielding zone near the oxirane, and 5-H_S is in the deshielding zone around the oxirane C-O bond, the reverse of the arrangement in the global minimum. Also, 5-H_S is in the deshielding zones of Phe 119 and Trp 37, which reinforce the oxirane deshielding effect.

We also determined the spin-lattice relaxation time, T_1, and the transverse relaxation time T_2 for the two 5-D signals and the combined 6-D signals (Figure 7), to better understand how the hydrogen atoms at the 5 and 6 positions of the disparlure enantiomers interact locally with the two binding proteins.

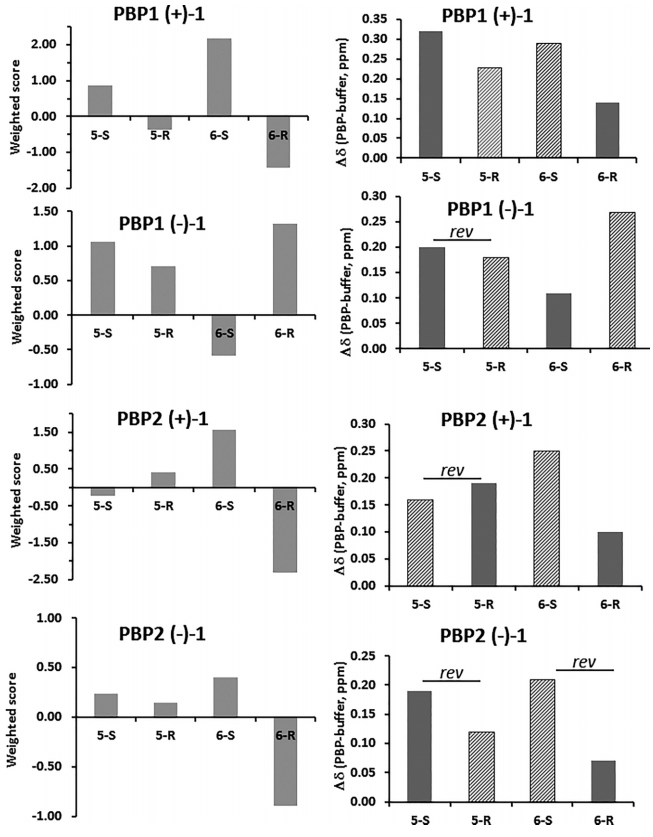

Figure 5. Left: weighted scores for shielding (< 0) or deshielding (> 0) effects, from docking simulations, weighted for distribution of poses at the internal and the two external sites and weighted for the distribution of the ligand between external and internal sites as shown in Table 7. Right: chemical shift differences (Δδ) between disparlure bound to PBP and disparlure in buffer. The hatched bars correspond to the signal labelled D_a and the dark gray bars correspond to the signal labelled D_b. Bars labelled "rev" exhibited a reversed assignment of prochirality for the D_a and D_b signals, relative to the assignment in an isotropic medium (Table 4).

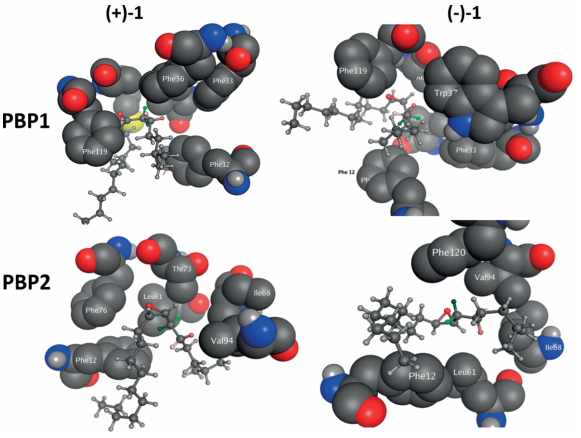

Figure 6. Interactions at the internal binding site of the most populated pose for each combination of protein and ligand. Top row: PBP1, bottom row: PBP2. The disparlure chain is shown in ball-and-stick format, with the epoxide colored red, 6-H_S = light green, 6-H_R = dark green, 5-H_S light pink, 5-H_R = dark pink. Residues that have a part interacting with any of the focal hydrogen atoms within a 4.5 Å radius are shown in space-filling format, without their hydrogen atoms.

T_1 reflects the longitudinal relaxation of the magnetic field in the z direction to its equilibrium value. This process is influenced by the local fluctuations in the magnetic field around the nucleus being observed. The frequencies of these fluctuations depend on the local density of the medium around the nucleus: the greater the density and viscosity (i.e. the lower the mobility), the larger T_1.[32] The transverse relaxation process reflects the decay of the phasing of nuclei in the xy plane. It depends on the fluctuations in the local magnetic field and on spin exchange between neighboring nuclei of opposite spin. In the gas phase, the local fluctuations average and $2T_1 \cong T_2$. At increasing viscosity in a condensed phase, the local magnetic fluctuations do not average, spin exchange occurs and T_2 decreases.[32]

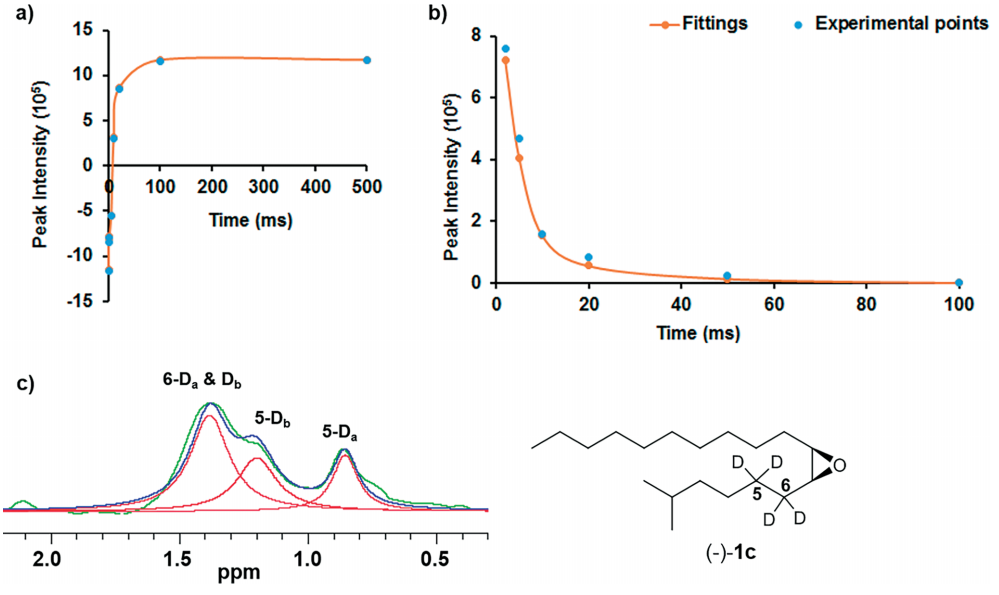

Figure 7. Determination of relaxation times T_1 and T_2. **a)** Example of a T_1 determination for 5-D_a of (–)-**1c** with *Ldis* PBP1 (phosphate buffer, pH 8) by following the re-establishment of the magnetization after a 90° pulse (see Figure S9 for traces) **b)** Example of a T_2 determination for 5D_a of **(–)-1c** with *Ldis* PBP1 (phosphate buffer, pH 8) by following the decay of the signal intensity after a 180° pulse. c) Example of signal deconvolution for 5-D_a, 5-D_b and 6-$D_{a/b}$.

Thus, the two relaxation times give insight into the mobility around the focal nucleus. In our molecular models, we checked the number of interactions between the focal hydrogen atoms and groups either on the protein or the twisted chain of disparlure. All interactions within a 4 Å radius were counted, and an estimate of the local mobility was obtained as the inverse of that number of interactions. This was done for each retained pose at each of the three sites, and mobility was averaged for each site and across sites, as described in the experimental and supplemental information. The inverse of the averaged mobility is a measure of the local viscosity: the more interactions, the lower the mobility and the higher the local viscosity.

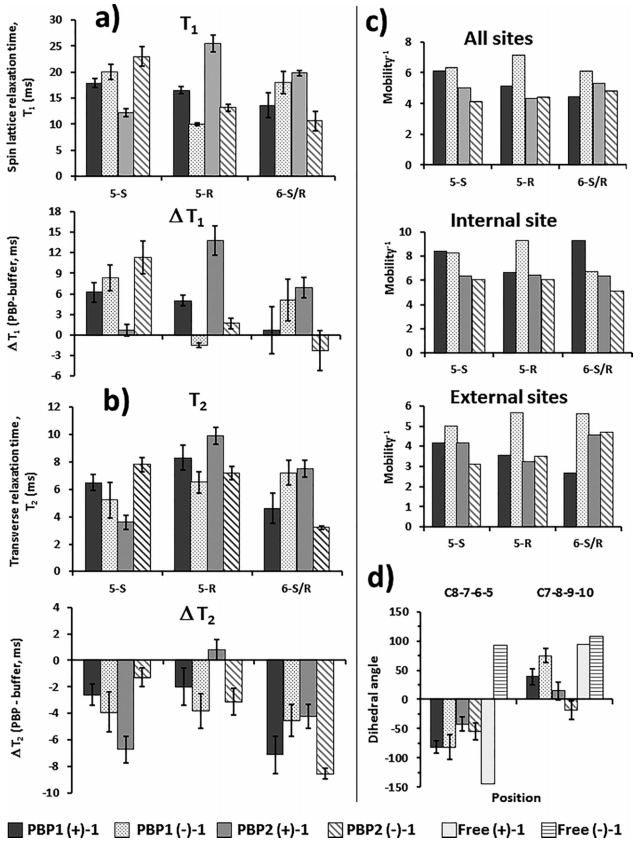

Figure 8. Left: spin relaxation data from ^{2}H NMR experiments with PBP1 and PBP2 with **(+)-1** or **(–)-1** bound. Right: measurements obtained from docking simulations of the ligands into one internal and two external sites on PBP1 and PBP2. Dark gray = PBP1 and **(+)-1**, stippled = PBP1 and **(–)-1**, medium gray = PBP2 and **(+)-1**, hatched = PBP2 and **(–)-1**. **a**) Top: Spin lattice relaxation time,T_1, in ms. Bars represent the average value from fitting of decay data, and the error bars denote the fitting error. Bottom: difference in T_1 between PBP-bound ligand and the ligand in buffer. Error bars are the sum of both errors. **b)** Top: transverse relaxation time,T_2, in ms. Bars represent the average value from fitting of decay data, and the error bars denote the fitting error. Bottom: difference in T_2 between PBP-bound ligand and the ligand in buffer. Error bars are the sum of both errors. **c)** Inverse mobility (which is approximately the average number of interactions and is proportional to the local viscosity) detected at all three sites (weighted for population of the sites – see text), at the internal site and at the two external sites (average of both sites). **d)** Average dihedral angles around C8–7–6–5 and C7–8–9–10, i.e. around the epoxide moiety. For the PBP-bound disparlure enantiomers the color scheme is the same as for the other graphs. Bars represent the weighted averages of all dihedral angles of retained poses, weighted by pose at each site and by site distribution (see text). Error bars represent the S. D. The light gray bars represent the dihedral angles at the global minimum for **(+)-1** and the horizontally striped bars represent the dihedral angles at the global minimum for **(–)-1** as calculated in.[5]

Figure 7 shows an example of T_1 and T_2 determination for 5-D_a of **(–)-1c** in the presence of *Ldis* PBP1 (phosphate buffer, pH 8). The T_1 values for the four combinations of PBP and disparlure enantiomers are shown in Figure 8a and Table 8. Because $CDCl_3$ and buffer are non-chiral, isotropic media, we only performed the measurements with one of the two enantiomers, **(–)-1c**. It is interesting to note that both solvent systems gave the same T_1 values within limits of error. In buffer, the signals were much weaker than in $CDCl_3$ or in the protein-bound cases (Figure 3), because in buffer disparlure has a strong tendency to adsorb on the walls of the vial. Signal from adsorbed disparlure is not detectable, since its mobility is completely restricted and T_1 is very long, T_2 is very short, both outside of the range of this experiment. Thus, in buffer, we detected only the disparlure that was dissolved in the aqueous phase.

Comparing T_1 values obtained for PBP-bound disparlure enantiomers and the value obtained for the free disparlure in solvent (Figure 8a) we see that, in general, there was an increase in T_1 upon binding of disparlure to the PBPs. This suggests that, generally, the mobility of the focal hydrogen atoms decreased upon binding to the protein. However, the signal intensity increased relative to buffer (Figure 3), and this is because PBPs help to desorb pheromones from solid surfaces, thus brining the hydrophobic pheromone into solution.[3,30] Exceptions to the general increase in T_1 upon protein binding were: 5-H_S in PBP2 with **(+)-1c**, 6-$H_{S/R}$ in PBP1 with **(+)-1c** and 6-$H_{S/R}$ in PBP2 with **(–)-1c**, all of which did not differ from the T_1 value seen in buffer. Thus, for these exceptional cases the local viscosity around the focal hydrogen atom in the protein-bound ligand was the same as that of free ligand.

The site-averaged inverted mobility patterns obtained from modelling (Figure 8c) parallel the patterns seen for T_1 with the exception of 5-H_S in PBP2 with **(–)-1c**, 5-H_R in both PBP1 with **(–)-1c** and PBP2 with **(+)-1c**. For 5-H_S in PBP2 with **(–)-1c** the inverted mobility (local viscosity) was lower than reflected in the T_1. Interaction at the internal binding site between 5-H_S and the two methyl groups of the side chain of Val 94 (both within van der Waals radius) contributes to restriction in the mobility of 5-H_S much more than is estimated by simple counting of interactions. Similarly, for 5-H_R in PBP2 with **(+)-1c**, the methyl groups of Val 94 or of Leu 52 clamp around that hydrogen atom in the three most populated poses at the internal binding site.

Additionally, methyl groups or Ile 68 and Thr 73 also surround that hydrogen atom in those internal poses. Conversely, 5-H_R of PBP1 with **(–)-1c** only has weak interactions with Phe 36 and Phe 119 on the protein and intramolecular interactions with 7-H, 3-H_S and 2-H. Counting these interactions overestimates their contribution to the relative local viscosity.

Comparing T_2 values obtained for PBP-bound disparlure enantiomers and the value obtained for the free disparlure in solvent (Figure 8b, Table 9) we see that, in general, there was a decrease in T_2 upon binding of disparlure to the PBPs. This suggests that, generally, the mobility of the focal hydrogen atoms decreased upon binding to the protein, consistent with the conclusion from T_1 data. The only case in which T_2 in the

Table 8. Spin-lattice relaxation (T_1) of 5,6-D_4 (+)-**1c** and (–)-**1c** in $CDCl_3$, buffer and PBP-bound.

Condition	5-D_a		5-D_b		6-D_a & 6-D_b	
	(+)-1c	**(–)-1c**	**(+)-1c**	**(–)-1c**	**(+)-1c**	**(–)-1c**
$CDCl_3$		13.6 ± 2.6		12.7± 0.7		11.6 ± 1.5
Phosphate buffer		11.5 ± 0.1		11.7 ± 0.5		12.9 ± 1.0
Buffer+ *Ldis*PBP1	16.5 ± 0.7	10.0 ± 0.2	17.9 ± 0.9	20.05 ± 1.42	13.6 ± 2.4	18.0 ± 2.1
Buffer+ *Ldis*PBP2	12.2 ± 0.7	13.2 ± 0.7	25.5 ± 1.6	23.0 ± 1.9	19.8 ± 0.5	10.6 ± 1.9

Table 9. Spin-spin (transverse) relaxation (T_2) of 5,6-D_4 (+)-**1c** and (–)-**1c** in the presence and absence of *Ldis*PBPs.

Condition	5-Da		5-Db		6-Da & 6-Db	
	(+)-1c	**(–)-1c**	**(+)-1c**	**(–)-1c**	**(+)-1c**	**(–)-1c**
$CDCl_3$		12.0 ± 0.1		11.4 ± 0.6		10.2 ± 0.1
Phosphate buffer		10.3 ± 0.5		9.1 ± 0.2		11.7 ± 0.3
Buffer+ *Ldis*PBP1	8.3 ± 0.9	6.5 ± 0.8	6.5 ± 0.6	5.2 ± 1.3	4.6 ± 1.1	7.2 ± 0.9
Buffer+ *Ldis*PBP2	3.6 ± 0.5	7.2 ± 0.5	9.9 ± 0.6	7.8 ± 0.5	7.5 ± 0.6	3.2 ± 0.1

protein-bound disparlure and the solvent did not differ was 5-H_R in PBP2 with **(+)-1**. This is interesting, because we know from T_1 and the modelling that 5-H_R in this case is very strongly restricted in its mobility at the internal binding site, so T_2 should be short and not detected. From kinetic data we know that, for PBP2, once disparlure is bound internally it dissociates only very slowly (with a rate constant of $4.7 \pm 0.4 \times 10^{-4}$ s^{-1}),[4] too slow for T_2 to be detectable in the current experiment. At the external sites in this case, interactions with 5-H_R in PBP2 with **(+)-1** are weak, and anisotropic effects cancel each other, so fluctuations in the magnetic field would be averaged as they would in a solvent.

Another interesting case is 6-$H_{S/R}$ in PBP1 with **(+)-1**, in which T_2 decreased significantly relative to solvent but T_1 was no different than in solvent. This pattern can be explained by a high number of interactions with 6-$H_{S/R}$ at the internal binding site. PBP1 associates with and dissociates from ligand much faster than PBP2, so that internal binding contributions would be detectable in the pattern of T_2. PBP1 binds **(+)-1** more weakly than **(–)-1**, at internal[3,33] and external (this study) binding sites. Thus, for PBP1 and the two enantiomers, the T_2 pattern is likely dominated by contributions from internal binding, and the inverted mobility pattern (or local viscosity) (Figure 8c) perfectly explains the T_2 pattern: more viscosity (lower T_2) for **(+)-1** and lower local viscosity (higher T_2) for **(–)-1**.

Finally, the case of 6-$H_{S/R}$ in PBP2 with **(–)-1** is also interesting. The T_1 for this case did not change significantly from solvent (Figure 8a), but T_2 significantly decreased upon protein binding (Figure 8b). In external site 2 of PBP2, the Lys 2 ε-NH_3^+ is H-bonded to the epoxide of **(–)-1** and the δ-CH_2 of Lys 2 packs near 6-H_S in the model. Both 6-H_S and 6-H_R pack with the β-CH_2 of Asp 132. These interactions could restrict mobility of the 6-$H_{S/R}$ of **(–)-1**, such that the T_2 value detected is shorter than the one detected with **(+)-1**, which does not interact in that way with site 2 of PBP2.

PBP1 only had a significant difference in T_1 between bound enantiomers of disparlure at 5-H_R, whereas PBP2 showed enantiomer differences at 5-H_S, 5-H_R and 6-$H_{S/R}$ (Figure 8a). For T_2, PBP1 showed significant differences between enantiomers for 5-H_R and 6-$H_{S/R}$, and PBP2 again showed significant differences between enantiomers for all three signals (Figure 8b). This is consistent with the body of previous studies on PBP1 and PBP2 interactions with the enantiomers of disparlure. PBP1 interacts more weakly overall but with greater differences in equilibrium dissociation constants than PBP2,[3,5,6,33] and PBP1 associates with and dissociates from disparlure enantiomers faster and more selectively than PBP2.[4,18] The slower kinetic regime followed by PBP2 is consistent with the greater number of significant differences between enantiomers in T_1 and T_2 detected here. PBP1 binds **(–)-1** more strongly at equilibrium than **(+)-1**, and PBP2 is the opposite.[3,5,33] Taken together, the chemical shift, T_1 and T_2 data, along with the models, demonstrate that the PBPs discriminate the disparlure enantiomers not only by binding differently to the epoxide moiety (Figure 8d), but also by interacting with subtle differences at positions 5 and 6, which were identified in 1977 as important general odotopes of disparlure in an electrophysiology structure-activity study with racemic disparlure analogs.[34]

Conclusion

In conclusion, a concise and efficient synthetic route to bioactive (+)-disparlure, (–)-disparlure and isotope labelled disaprlure enantiomers was completed in high overall yields from commercially available dodecanal. Key steps in the synthesis involved MacMillan's SOMO-activated α-chlorination of the aldehyde, which was shown to be a highly effective means for preparing enantiopure α-chloroaldehyde (>99 % ee), and Mitsunobu inversion. Field tests showed that (+)-disparlure was very attractive. This is the first report on a study of interactions between isotope labelled disparlure enantiomers and *Ldis*PBPs of gypsy moth by using ^2H NMR spectroscopy. The present study confirms that the 5 and 6 positions on the hydrophobic short side chain of the disparlure enantiomers play an important role in recognition of the disparlure enantiomers in the binding site of the *Ldis*PBPs.

Experimental Section

General

All reactions were carried out in the presence of a nitrogen atmosphere and at room temperature (22 °C), unless the reactions were

performed in aqueous media or unless otherwise specified. Reactions carried out at –78 °C used a bath of dry ice in acetone. Reactions undertaken at 0 °C utilized a bath of water and ice. Hexanes and ethyl acetate were distilled prior to use. THF was distilled from sodium benzophenone. Chemicals and Reagents were used without further purification. Syringes and cannulas were used to transfer reagents. Reactions were monitored by thin layer chromatography (TLC) on aluminum baked silica plates (Merck Silica Gel 60 F254) and products were visualized under UV (λ = 254 nm) or stained with phosphomolybdic acid (PMA), anisaldehyde or potassium permanganate, followed by exposure of the stained plates to heat. Silica flash chromatography (Fisher Silica Gel 60 40–63 μm) was undertaken to purify crude reaction mixtures using hexanes/ethyl acetate mixture. The enantiomeric excess (ee) of 2-chlorododecyl benzoates **8** was analyzed on an Agilent 1100 HPLC equipped with a chiral Lux 5μm Cellulose-2 column (Phenomenex) and variable wavelength detector (VWD). The HPLC chromatograph was programmed isocratically with hexanes/2-propanol (99:1). Optical rotations were recorded on a Perkin–Elmer Polarimeter 340 thermostatted to 20 °C, using the sodium D line.

The ^{1}H NMR spectra were obtained on Bruker DRX 400 and 500 MHz spectrometers in $CDCl_3$. Chemical shifts and coupling constants are reported in parts per million (ppm) and Hertz (Hz) respectively. ^{1}H NMR data was reported as follows: chemical shift values (ppm), multiplicity (s = singlet, d = doublet, t = triplet, q = quartet, m = multiplet). ^{13}C NMR spectra were recorded in $CDCl_3$ by using a Bruker DRX 400 or DRX 500. ^{13}C NMR data was reported as chemical shift values (ppm). IR spectra were obtained with a Perkin–Elmer Spectrum One FT-IR spectrometer and samples were directly placed on the KBr plates. High-resolution mass spectra (HRMS) were obtained by using positive electrospray ionization and by TOF method. Syringes and cannulas were used to transfer reagents. The GC–MS analysis was performed on GC–MS (Varian *CP*3800 GC, interfaced with a Varian Saturn 2000 MS) using a SPB-5 fused silica capillary column (30 m × 0.25 mm i.d., film thickness 0.25 μm, Supelco, Bellefonte, PA, USA) with positive electron ionization (EI), and final GC–MS analysis was done on a Perkin Elmer Clarus 690 GC with a Elite-5MS (30 m × 0.25 mm i.d., film thickness 0.25 μm) column, interfaced with a SQ8T quadrupole mass spectrometer. EI was the ionization mode, and He was the carrier gas.

Stopped-flow kinetics

Kinetics experiments were performed in a Chirascan stopped-flow instrument (Applied Photophysics Ltd, UK). For the competition kinetics, N-phenyl-1-naphthylamine (1-NPN) was used as the fluorescent reporter. First, the association and dissociation rate constants of 1-NPN were determined by association and the values were used as constraints for calculating the k_{on} and k_{off} of the ligands. In the competitive assay, one reservoir was filled with the PBP1 solution (0.50 μM PBP1 in 20 mM Tris/HCl buffer pH 8.0 with 180 mM KCl, 25 mM NaCl, and 0.1 % ethanol) while the second reservoir contained the solution of NPN (0.50 μM) mixed with various concentrations of **(+)-1c** or **(–)-1c** in the same buffer. The NPN was added from a 0.50 mM NPN in methanol stock. Six microliters of **(+)-1c** or **(–)-1c** was added from stock solutions in ethanol (0.20 mM to 1.6 mM). The stopped-flow instrument mixed the solutions in 1:1 volume ratio from the two reservoirs. The final concentrations of the participating components were the following: (1) PBP1 0.25 μM, (2) NPN 0.25 μM, and (3) **(+)-1c** or **(–)-1c** 0 to 9.4 μM. NPN fluorescence was observed using 337 nm excitation and the emission detected using longpass filter disc with 395 nm cutoff. The experiment was performed at constant temperature, 22 °C. The fluorescent traces were fitted using kinetics of competitive binding model in GraphPad Prism 5 (GraphPad Software Inc., California).

Sample preparation for T_1 and T_2 relaxation experiments

The stock solutions of poorly water soluble deuterated disparlure enantiomers were prepared by dissolving in acetonitrile. 50 mM phosphate buffer of pH 8 was prepared by using mono and dibasic sodium phosphate. The protein (*Ldis*PBPs) solutions (0.3 mM) were incubated with deuterium labelled disparlure enantiomers (0.6 mM) in ice cold water for 3 h. The protein-ligand interaction process was monitored through acquisition of ^{2}H NMR spectra. The ^{2}H NMR relaxation spectra of the deuterated disparlure enantiomers/*Ldis*PBPs system were obtained using a Bruker –600 NMR spectrometer equipped with QCI probe. The T_1 (relaxation) times were measured by using with the standard inversion-recovery pulse sequence[35] (180° – τ - 90°). The T_2 (transverse relaxation) times were measured using with Carr-Purcell-Meiboom-Gill pulse sequence[36] (90° (τ-180° – τ) $_n$). The delay times in between 180° were used as 0.42 ms. T_1 and T_2 relaxation curves were fitted to Equation 1 and Equation 2, respectively.

$$M_z(t) = M_z(0)\ (1 - \exp\ (-t/T_1) \quad (1)$$

$$M_{xy}(t) = M_{xy}(0)\ (\exp\ (-t/T_2) \quad (2)$$

Homology models of *Ldis*PBP1 and *Ldis*PBP2

Gypsy moth PBP1 and PBP2 share 61.7 % and 48.9 % similarity with Bombyx *mori* PBP, respectively. The homology models of *Ldis*PBP1 and *Ldis*PBP2 were created based on the crystal structure of Bombyx *mori* PBP (PDB ID: 1LS8.1. A) by using SWISS MODEL (expasy.org).[37,38] The models were corrected for lacking hydrogen atoms, using the "Protonate 3D" function in Molecular Operating Environment (MOE, Chemical Computing Group, Montreal, Canada) at pH 8 and with 0.10 M salt concentration. Using the MMFF94X force field, the "protonate 3D" function assigns the location of hydrogen atoms and ionization states in the protein structure. After protonation, energy minimization was applied to the protein structures.

Molecular docking simulations

The homology models were docked with disparlure enantiomers by using an induced fit protocol. Docking stimulations were performed with the MMFF94X force field in MOE, using default parameters (Refinement: Force field, Placement: Triangle Matcher). Two scoring functions (Rescoring 1: London dG and Rescoring 2: GBVI/WSA dG) were used for this docking protocol. The ligand binding sites of protein were detected in MOE by using geometric algorithm based on Edelsbrunner's Alpha Shapes called "Site Finder" in MOE.[39]

Evaluation of molecular docking simulation data

The simulations were programmed such that the fit of the ligand into the binding site was induced and up to 30 poses of the ligand were retained. We obtained between 18 and 30 poses, which were evaluated for the total potential energy. Using the assumption that all the poses can equilibrate with the pose of lowest energy, a distribution of poses was calculated for each case (see supplemental information).

Next, all poses that were found to be populated above 5 % were examined with regard to molecular interactions with the epoxide and the 5_S, 5_R, 6_S and 6_R hydrogen atoms. To perform this inspection, binding pocket residues and functional groups within a 4.5 Å of the focal atoms were selected. Distances of nearby hydrogen atoms to the 5 and 6 H atoms were measured, both on the protein and on disparlure itself. We also checked whether the focal hydrogen atoms are within the shielding or deshielding zones of nearby phenyl or indole systems of phenylalanine or tryptophan residues or of carbonyl groups (in the backbone or aspartate,

glutamate, asparagine or glutamine side chains). We also assessed every focal hydrogen atom with regard to its position relative to the oxirane ring's shielding and deshielding zones.[40] The interactions found were tabulated and scored according to the following scale: 0 = neither shielding nor deshielding; –1 = weak shielding; 1 = weak deshielding; –2 moderate shielding; 2 = moderate deshielding; –3 = strong shielding; 3 = strong deshielding. This assessment was performed for each enantiomer in each relevant retained pose (populated > 5 %). Weighted averages were calculated for each enantiomer at each site.

Finally, a global weighting was done for internal and external sites, taking into consideration that the ligand can partition between external sites and the internal one, according to previous kinetic binding experiments,[4] and overall equilibrium binding constants determined recently at pH 8.0.[33] The overall binding constants determined at equilibrium were taken to reflect the affinity of the proteins for internally bound ligands. Affinity of the external sites for the ligands was determined here for PBP1, using a fluorescent displacement assay in a stopped-flow apparatus and from our previous study[4] for PBP2. Dissociation constants for external binding were estimated as k_{off}/k_{on}, the ratio of the dissociation and association rate constants. Shielding and deshielding contributions from the three sites were weighted according to the percentages shown in Table 7.

Synthetic procedures

General procedure for Preparation of (+)-3 and (–)-3

To a cold (0 °C), stirred suspension of lithium chloride (0.016 mol) in acetonitrile (50 mL), was added copper (II) trifluoroacetate hydrate (0.004 mol) and sodium persulfate (0.004 mol) followed by H_2O (0.017 mol). The reaction mixture was stirred for 5 min and then the SOMO catalyst ((2*S*, 5*R*)-2-(*tert*-butyl)-3,5-dimethylimidazolidin-4-one or (2*R*, 5*S*)-2-(*tert*-butyl)-3,5-dimethylimidazolidin-4-one 0.0016 mol) was added. After stirring for 5 min at 0 °C, dodecanal (0.008 mmol) was added. The reaction mixture was stirred for 1 h and then allowed to slowly warm to 5 °C over the course of 24 h. The mixture was stirred at 5 °C until dodecanal had been completely consumed (as determined by ^{1}H NMR spectroscopy). After this time, the reaction mixture was treated with water (20 mL) and diluted with ethyl acetate (50 mL), and the phases were separated. The aqueous phase was extracted with ethyl acetate (3×50 mL) and the combined organic phases were washed with brine (20 mL), dried with $MgSO_4$, and concentrated to give the crude chloroaldehyde. Purification of the crude product by flash chromatography afforded the desired products.

(+)-(2*R*)-2-Chlorododecanal (+)- 3

(Eluent: 1 % EA/hexane), 1.03 g, 87 %, pale yellow oil: ^{1}H NMR (500 MHz, $CDCl_3$) δ: 9.48 (d, 1H, *J* = 2.5 Hz), 4.15 (ddd, 1H, *J* = 8.5 Hz, 5.5 Hz, 3 Hz), 1.99–1.92 (dddd, 1H, *J* = 16 Hz, 11.5 Hz, 10.5 Hz, 6Hz), 1.84–1.78 (dddd, 1H, *J* = 18.5 Hz, 14 Hz, 8.5 Hz, 5 Hz), 1.54–1.48 (m, 1H), 1.44–1.37 (m, 1H), 1.25 (m, 14H), 0.88 (t, 3H, *J* = 7 Hz). ^{13}C NMR (500 MHz, $CDCl_3$) δ: 194.7, 63.4, 31.4, 31.3, 28.9, 28.8, 28.7, 28.3, 24.9, 22.0, 13.5. IR (neat): ṽ = 2955, 2925, 2855, 2718, 1736, 1466, 759 cm^{-1}. HRMS (ESI) *m/z* calculated for $C_{12}H_{23}ClO$ [M – H] 217.1359, found 217.1362. $[\alpha]^{25}_{D:}$ +10 (c 0.5, $CHCl_3$).

(–)-(2*S*)-2-Chlorododecanal (–)-3

(Eluent: 1 % EA/hexane), 1.0 g, 84 %, pale yellow oil: ^{1}H NMR (500 MHz, $CDCl_3$) δ: 9.48 (d, 1H, *J* = 2.5 Hz), 4.17–4.14 (ddd, 1H, *J* = 8.5 Hz, 5.5 Hz, 3 Hz), 2.02–1.93 (dddd, 1H, *J* = 16 Hz, 11.5 Hz, 10.5 Hz, 6Hz), 1.86–1.77 (dddd, 1H, *J* = 18.5 Hz, 14 Hz, 8.5 Hz, 5 Hz), 1.68–1.57 (m, 1H), 1.53–1.39 (m, 1H), 1.26 (m, 14H), 0.87 (t, 3H, *J* = 7 Hz). ^{13}C NMR (500 MHz, $CDCl_3$) δ: 195.3, 63.8, 31.9, 31.7, 29.4, 29.3, 29.1, 28.8, 25.4, 22.6, 14.0. IR (neat): ṽ = 2957, 2928, 2855, 2718, 1738, 1466, 759 cm^{-1}. HRMS (ESI) *m/z* calculated for $C_{12}H_{23}ClO$ [M – H] 217.1359, found 217.1362. $[\alpha]^{25}_{D:}$ –9.9 (c 0.5, $CHCl_3$).

General procedure for Preparation of (+)-4 and (–)-4

To a cold (–78 °C), stirred solution of 1-hexyne (0.015 mol) in THF (20 mL), a solution of *n*-butyllithium (2.5 M in hexanes, 0.014 mmol) was added dropwise. The resulting mixture was stirred at –78 °C for 1 h. After this time, a solution of (+)-**3** or (–)-**3** (0.008 mol) in THF (10 mL) was added dropwise and the reaction mixture was stirred for an additional 1 h. Then the reaction mixture was quenched with a saturated aqueous solution of NH_4Cl (10 mL), diluted with ethyl acetate (50 mL) and water (20 mL). The phases were separated, and the aqueous phase was extracted with ethyl acetate (3×50 mL). The combined organic layers were washed with brine (30 mL), dried with $MgSO_4$, and concentrated under reduced pressure, which afforded crude product (dr. 20:1 determined by ^{1}H NMR analysis of the crude reaction mixture). Purification of the crude product by flash chromatography afforded (silica gel, 95:5 hexanes/ethyl acetate) yielded (+)-**4 or** (–)-**4**.

(7*S*, 8*R*)-8-Chloro-2-methyloctadec-5-yn-7-ol (+)-4

(Eluent: 5 % EA/hexane), 1.94 g, 89 %, pale yellow oil: ^{1}H NMR (500 MHz, $CDCl_3$) δ: 4.50 (dt, 1H, *J* = 3.6, 1.9 Hz), 4.0 (ddd, 1H, *J* = 9.3, 4.4, 3.5 Hz), 2.24 (td, 2H, *J* = 7.4 Hz, 2.0 Hz),1.82 (m, 2H),1.70 (m, 1H),1.56 (m, 2H),1.27 (m, 17H), 0.90 (d, 6H, *J* = 6.6 Hz), 0.89 (t, 3H, *J* = 7 Hz). ^{13}C NMR (500 MHz, $CDCl_3$) δ: 87.9, 76.8, 67.6, 66.4, 37.5.6, 33.7, 32.0, 29.7, 29.5, 29.4, 29.2, 27.3, 26.6, 22.8, 22.2, 16.8, 14.2. IR (neat): ṽ = 3416, 2956, 2926, 2855, 2237, 1466, 1042, 759 cm^{-1}. HRMS (ESI) *m/z* calculated for $C_{18}H_{33}ClONa$ [M + Na]: 337.2274, found 337.1042.

(7*R*, 8*S*)-8-Chloro-2-methyloctadec-5-yn-7-ol (–)-4

(Eluent: 5 % EA/hexane), 1.88 g, 86 %, pale yellow oil: ^{1}H NMR (500 MHz, $CDCl_3$) δ: 4.50 (dt, 1H, *J* = 3.6, 1.9 Hz), 4.03–3.99 (ddd, 1H, *J* = 9.3, 4.4, 3.5 Hz), 2.26–2.22 (td, 2H, *J* = 7.4 Hz, 2.0 Hz),1.88–1.75 (m, 2H),1.72–1.66 (m, 1H),1.63–1.52 (m, 2H),1.26 (m, 17H), 0.90 (d, 6H, *J* = 6.6 Hz), 0.86 (t, 3H, *J* = 7 Hz). ^{13}C NMR (500 MHz, $CDCl_3$) δ: 87.7, 76.8, 67.4, 66.2, 37.5.6, 33.5, 31.8, 30.4, 29.5, 29.3, 29.2, 29.0, 26.3, 22.6, 21.8, 18.2, 14.0, 13.4. IR (neat): ṽ = 3417, 2957, 2926, 2855, 2237, 1466, 1042, 759 cm^{-1}. HRMS (ESI) *m/z* calculated for $C_{18}H_{33}ClONa$ [M + Na]: 337.2274, found 337.1042.

General procedure for Preparation of (+)-5, (+)-5a, (+)-5b, (+)-5c, (–)-5, (–)-5b and (–)-5c

To an ice cold, stirred solution of triphenylphosphane (0.0082 mol) in dry THF (20 mL), benzoic acid or ^{17}O or ^{18}O benzoic acid (0.0082 mol) and the solution of (+)-**4** or (–)-**4** (0.0041 mol) in dry THF (10 mL) were added slowly to the reaction flask under an inert N_2 atmosphere. The resulting mixture was stirred at 0 °C for 5 minutes. After this time, a solution of diisopropyl azodicarboxylate (0.0082 mol) in dry THF (5 mL) was added dropwise and the reaction mixture was stirred at room temperature for 12 h. The reaction solvent was removed by evaporation under reduced pressure and diluted with ethyl acetate (50 mL) and water (20 mL). The phases were separated, and the aqueous phase was extracted with ethyl acetate (3 × 50 mL). The combined organic layers were washed with brine (20 mL), dried with $MgSO_4$, and concentrated under reduced pressure, which afforded crude product. Purification of the crude product by flash chromatography (silica gel, 99:1 hexanes/ethyl acetate) afforded the desired target compounds.

(7*R*, 8*R*)-8-Chloro-2-methyloctadec-5-yn-7-yl benzoate (+)-5

(Eluent: 1 % EA/hexane), 1.37 g, 80 %, pale yellow oil: ^{1}H NMR (500 MHz, $CDCl_3$) δ: 8.09 (d, 2H, *J* = 7.2 Hz), 7.58 (t, 1H, *J* = 7.4 Hz), 7.46 (t, 2H, *J* = 7.7 Hz), 5.74 (dt, 1H, *J* = 6.1 Hz, 1.9 Hz), 4.09 (ddd, 1H, *J* = 9.6 Hz, 6.2 Hz, 3.4 Hz), 2.24 (td, 2H, *J* = 7.4 Hz, 1.9 Hz), 2.02 (m, 1H), 1.84 (m, 1H), 1.66 (m, 2H), 1.43 (dd, 2H, *J* = 14.5 Hz, 7.3 Hz), 1.26 (m, 14H), 1.16 (m, 2H), 0.89 (t, 3H, *J* = 6.3 Hz), 0.88 (d, 6H, *J* = 6.6 Hz). ^{13}C NMR (500 MHz, $CDCl_3$) δ: 165.1, 133.3, 130.0, 129.5, 128.5, 88.7, 77.1, 74.4, 67.8, 62.5, 37.2, 33.8, 32.0, 29.7, 29.6, 29.5 29.4, 29.1, 27.3, 26.1 22.7, 22.2, 16.8, 14.2. IR (neat): $\tilde{\nu}$ = 2941, 2879, 2238, 1727, 1261, 1103, 1093, 956, 708 cm^{-1}. HRMS (ESI) *m/z* calculated for $C_{26}H_{39}ClO_2$ [M + H]: 419.2701, found 419.2696. $[\alpha]_D^{25}$: + 5.7 (c 0.8, CCl_4).

(7*R*, 8*R*)-8-Chloro-octadec-5-yn-7-yl benzoate (+)-5a

(Eluent: 1 % EA/hexane), 1.25 g, 73 %, pale yellow oil: ^{1}H NMR (500 MHz, $CDCl_3$) δ: 8.09 (d, 2H, *J* = 7.2 Hz), 7.58 (t, 1H, *J* = 7.4 Hz), 7.46 (t, 2H, *J* = 7.7 Hz), 5.74 (dt, 1H, *J* = 6.1 Hz, 1.9 Hz), 4.09 (ddd, 1H, *J* = 9.6 Hz, 6.2 Hz, 3.4 Hz), 2.24 (td, 2H, *J* = 7.4 Hz, 1.9 Hz), 2.02 (m, 1H), 1.84 (m, 1H), 1.66 (m, 2H), 1.43 (dd, 2H, *J* = 14.5 Hz, 7.3 Hz), 1.26 (m, 14H), 1.16 (m, 2H), 0.89 (t, 3H, *J* = 6.3 Hz), 0.87 (t, 3H, *J* = 5.9 Hz). ^{13}C NMR (500 MHz, $CDCl_3$) δ: 165.1, 133.3, 130.0, 128.5, 88.7, 77.1, 74.4, 67.8, 62.5, 37.2, 33.8, 32.0, 29.7, 29.6, 29.5 29.4, 29.1, 27.3, 26.1 22.7, 22.2, 16.8, 14.2. IR (neat): $\tilde{\nu}$ = 2941, 2879, 2238, 1727, 1261, 1103, 1093, 956, 708 cm^{-1}. $[\alpha]_D^{25}$: + 5.7 (c 0.8, CCl_4).

(7*R*, 8*R*)-8-Chloro-2-methyloctadec-5-yn-7-yl benzoate-$^{17}O_2$ (+)-5b

Triphenylphosphane (0.00127 mol), ^{17}O benzoic acid (0.00127 mol) and (+)-**4** (0.000636 mol). (Eluent: 1 % EA/hexane), 0.208 g, 78 %, pale yellow oil: ^{1}H NMR (500 MHz, $CDCl_3$) δ: 8.09–8.08 (d, 2H, *J* = 7.2 Hz), 7.60–7.57 (t, 1H, *J* = 7.4 Hz), 7.47–7.44 (t, 2H, *J* = 7.7 Hz), 5.75–5.74 (dt, 1H, *J* = 6.1 Hz, 1.9 Hz), 4.12–4.08 (ddd, 1H, *J* = 9.6 Hz, 6.2 Hz, 3.4 Hz), 2.26–2.23 (td, 2H, *J* = 7.4 Hz, 1.9 Hz), 2.07–2.00 (m, 1H), 1.88–1.80 (m, 1H), 1.70–1.65 (m, 1H), 1.26 (m, 18H), 0.89 (t, 3H, *J* = 6.3 Hz), 0.87 (d, 6H, *J* = 6.6 Hz). ^{13}C NMR (500 MHz, $CDCl_3$) δ: 165.05, 165.02 ($^{13}C_{benzoate}$-^{17}O), 133.2, 129.8, 129.5, 128.3, 88.4, 77.1, 74.2, 67.7, 67.6 ($^{13}C_{benzoate}$-^{17}O), 62.4, 37.1, 33.6, 31.8, 29.5, 29.4, 29.3 29.2, 28.9, 27.1, 25.9 22.6, 22.0, 16.7, 14.0. IR (neat): $\tilde{\nu}$ = 2947, 2882, 2238, 1727, 1261, 1103, 1093, 956, 708 cm^{-1}. $[\alpha]_D^{25}$: + 5.7 (c 0.8, CCl_4).

(7*R*, 8*R*)-8-Chloro-2-methyloctadec-5-yn-7-yl benzoate-$^{18}O_2$ (+)-5c

Triphenylphosphane (0.00127 mol), ^{18}O benzoic acid (0.00127 mol) and (+)-**4** (0.000636 mol). (Eluent: 1 % EA/hexane), 0.213 g, 80 %, pale yellow oil: ^{1}H NMR (500 MHz, $CDCl_3$) δ: 8.09–8.08 (d, 2H, *J* = 7.2 Hz), 7.60–7.57 (t, 1H, *J* = 7.4 Hz), 7.47–7.44 (t, 2H, *J* = 7.7 Hz), 5.75–5.73 (dt, 1H, *J* = 6.1 Hz, 1.9 Hz), 4.12–4.08 (ddd, 1H, *J* = 9.6 Hz, 6.2 Hz, 3.4 Hz), 2.25–2.22 (td, 2H, *J* = 7.4 Hz, 1.9 Hz), 2.06–2.02 (m, 1H), 1.88–1.80 (m, 1H), 1.70–1.65 (m, 1H), 1.30–1.26 (m, 18H), 0.89 (t, 3H, *J* = 6.3 Hz), 0.87 (d, 6H, *J* = 6.6 Hz). ^{13}C NMR (500 MHz, $CDCl_3$) δ: 165.05, 165.03 ($^{13}C_{benzoate}$-^{18}O), 133.2, 129.8, 128.3, 88.4, 77.1, 74.2, 67.7, 67.6 ($^{13}C_{benzoate}$-^{18}O), 62.4, 37.1, 33.6, 31.8, 29.5, 29.4, 29.3 29.2, 28.9, 27.1, 26.0 22.6, 22.0, 16.7, 14.0. IR (neat): $\tilde{\nu}$ = 2945, 2879, 2238, 1727, 1261, 1103, 1093, 956, 708 cm^{-1}. HRMS (ESI) *m/z* calculated for $C_{26}H_{39}ClNa^{18}O_2$ [M + Na]: 443.2573, found 443.2574. $[\alpha]_D^{25}$: + 5.7 (c 0.8, CCl_4).

(7*S*, 8*S*)-8-Chloro-octadec-5-yn-7-yl benzoate (–)-5

(Eluent: 1 % EA/hexane), 1.30 g, 76 %, pale yellow oil: ^{1}H NMR (500 MHz, $CDCl_3$) δ: 8.09–8.07 (d, 2H, *J* = 7.2 Hz), 7.60–7.56 (t, 1H, *J* = 7.4 Hz), 7.46–7.44 (t, 2H, *J* = 7.7 Hz), 5.75–5.74 (dt, 1H, *J* = 6.1 Hz, 1.9 Hz), 4.12–4.07 (ddd, 1H, *J* = 9.6 Hz, 6.2 Hz, 3.4 Hz), 2.26–2.22 (td, 2H, *J* = 7.4 Hz, 1.9 Hz), 2.07–1.99 (m, 1H), 1.89–1.79 (m, 1H), 1.66 (m, 2H), 1.43 (dd, 2H, *J* = 14.5 Hz, 7.3 Hz), 1.26 (m, 14H), 0.89 (t, 3H, *J* = 6.3 Hz), 0.88 (d, 6H, *J* = 6.6 Hz). ^{13}C NMR (500 MHz, $CDCl_3$) δ: 165.1, 133.2, 130.0, 129.5, 128.3, 88.4, 77.1, 74.2, 67.7, 62.4, 37.1, 33.7, 32.0, 29.5, 29.4, 29.3 29.2, 29.0, 27.1, 26.0 22.6, 22.0, 16.7, 14.0. IR (neat): $\tilde{\nu}$ = 2941, 2879, 2238, 1727, 1261, 1103, 1093, 956, 708 cm^{-1}. HRMS (ESI) *m/z* calculated for $C_{26}H_{39}ClO_2$ [M + H]: 419.2701, found 419.2696. $[\alpha]_D^{25}$: - 5.67 (c 0.8, CCl_4).

(7*S*, 8*S*)-8-Chloro-octadec-5-yn-7-yl benzoate-$^{17}O_2$ (–)-5b

Triphenylphosphane (0.00127 mol), ^{17}O benzoic acid (0.00127 mol) and (–)-**4** (0.000636 mol). (Eluent: 1 % EA/hexane), 0.208 g, 78 %, pale yellow oil: ^{1}H NMR (500 MHz, $CDCl_3$) δ: 8.09–8.08 (d, 2H, *J* = 7.2 Hz), 7.60–7.56 (t, 1H, *J* = 7.4 Hz), 7.46–7.44 (t, 2H, *J* = 7.7 Hz), 5.76–5.73 (dt, 1H, *J* = 6.1 Hz, 1.9 Hz), 4.12–4.07 (ddd, 1H, *J* = 9.6 Hz, 6.2 Hz, 3.4 Hz), 2.26–2.23 (td, 2H, *J* = 7.4 Hz, 1.9 Hz), 2.07–1.99 (m, 1H), 1.89–1.79 (m, 1H), 1.71–1.63 (m, 1H), 1.26 (m, 18H), 0.89 (t, 3H, *J* = 6.3 Hz), 0.87 (d, 6H, *J* = 6.6 Hz). ^{13}C NMR (500 MHz, $CDCl_3$) δ: 165.0, 164.9 ($^{13}C_{benzoate}$-^{17}O), 133.1, 129.7, 129.5, 128.2, 88.3, 77.1, 74.2, 67.7, 67.6 ($^{13}C_{benzoate}$-^{17}O), 62.4, 37.0, 33.6, 31.8, 29.5, 29.4, 29.3 29.2, 28.9, 27.1, 25.9 22.6, 22.0, 16.7, 13.9. IR (neat): $\tilde{\nu}$ = 2947, 2882, 2238, 1727, 1261, 1103, 1093, 956, 708 cm^{-1}. $[\alpha]_D^{25}$: - 5.67 (c 0.8, CCl_4).

(7*S*, 8*S*)-8-Chloro-octadec-5-yn-7-yl benzoate-$^{18}O_2$ (–)-5c

Triphenylphosphane (0.00127 mol), ^{18}O benzoic acid (0.00127 mol) and (–)-**4** (0.000636 mol). (Eluent: 1 % EA/hexane), 0.213 g, 80 %, pale yellow oil: ^{1}H NMR (500 MHz, $CDCl_3$) δ: 8.10–8.07 (d, 2H, *J* = 7.2 Hz), 7.60–7.56 (t, 1H, *J* = 7.4 Hz), 7.48–7.44 (t, 2H, *J* = 7.7 Hz), 5.75–5.74 (dt, 1H, *J* = 6.1 Hz, 1.9 Hz), 4.12–4.07 (ddd, 1H, *J* = 9.6 Hz, 6.2 Hz, 3.4 Hz), 2.26–2.22 (td, 2H, *J* = 7.4 Hz, 1.9 Hz), 2.07–1.99 (m, 1H), 1.89–1.79 (m, 1H), 1.71–1.64 (m, 1H), 1.30–1.26 (m, 18H), 0.89 (t, 3H, *J* = 6.3 Hz), 0.87 (d, 6H, *J* = 6.6 Hz). ^{13}C NMR (500 MHz, $CDCl_3$) δ: 165.05, 165.03 ($^{13}C_{benzoate}$-^{18}O), 133.2, 129.8, 128.3, 88.4, 77.1, 74.2, 67.7, 67.6 ($^{13}C_{benzoate}$-^{18}O), 62.4, 37.1, 33.6, 31.8, 29.5, 29.4, 29.3 29.2, 28.9, 27.1, 26.0 22.6, 22.0, 16.7, 14.0. IR (neat): $\tilde{\nu}$ = 2945, 2879, 2238, 1727, 1261, 1103, 1093, 956, 708 cm^{-1}. HRMS (ESI) *m/z* calculated for $C_{26}H_{39}ClNa^{18}O_2$ [M + Na]: 443.2573, found 443.2574. $[\alpha]_D^{25}$: - 5.67 (c 0.8, CCl_4).

General procedure for Preparation of (+)-6, (+)-6a, (+)-6b, (+)-6c, (–)-6, (–)-6b and (–)-6c

A 100 mL round-bottomed flask was charged with methanol or benzene. The flask was evacuated and back filled with nitrogen gas. After two vacuum/nitrogen cycles to replace air with nitrogen inside the reaction flask, the compound (+)-**6** or (–)-**6** (0.0028 mol), 20 % Pd/C (240 mg, 20 wt.-% of compound) or $RhCl(PPh3)_3$ (10 mol-%) were added. The reaction mixture was vigorously stirred at room temperature under atmospheric hydrogen or deuterium pressure (balloon) for 3 h. After that the reaction mixture was filtered through a celite pad, and the filtrate was concentrated on a rotary evaporator to afford crude product. The crude product was carried to the next step without further purification.

(7*R*, 8*R*)-8-Chloro-2-methyloctadecan-7-yl benzoate (+)-6

Yield 1.14 g, 95 %, colorless oil: ^{1}H NMR (500 MHz, $CDCl_3$) δ: 8.09 (d, 2H, *J* = 7.2 Hz), 7.58 (t, 1H, *J* = 7.4 Hz), 7.45 (t, 2H, *J* = 7.7 Hz), 5.28 (dt, 1H, *J* = 7.2 Hz, 3.2 Hz), 4.06 (dt, 1H, *J* = 9.1 Hz, 4.0 Hz), 1.82 (m, 4H), 1.50 (m, 1H), 1.41 (m, 1H), 1.34 (m, 4H), 1.23 (m, 15H), 1.16 (m, 2H),0.87 (t, 3H, *J* = 6.3 Hz), 0.84 (d, 6H, *J* = 6.6 Hz). ^{13}C NMR (500 MHz, $CDCl_3$) δ: 166.0, 133.1, 130.0, 128.5, 75.7, 63.9, 38.7, 34.6, 32.0, 31.4, 29.6, 29.5, 29.4 29.3, 29.0, 27.9, 27.2, 26.7, 25.7, 22.7, 22.6, 22.5, 14.1. IR (neat): $\tilde{\nu}$ = 2945, 2880, 1721, 1266, 1108, 1069, 709 cm^{-1}. HRMS (ESI) *m/z* calcd. for $C_{26}H_{43}ClO_2$ [M + H]: 424.0792, found 424.2289. $[\alpha]_D^{25}$: +6.4 (c 0.68, CCl_4).

(7*R*, 8*R*)-8-Chloro-octadecan-7-yl benzoate (+)-6a

Yield 1.03 g, 86 %, colorless oil: ^{1}H NMR (500 MHz, $CDCl_3$) δ: 8.09 (d, 2H, *J* = 7.2 Hz), 7.58 (t, 1H, *J* = 7.4 Hz), 7.45 (t, 2H, *J* = 7.7 Hz), 5.28 (dt, 1H, *J* = 7.2 Hz, 3.2 Hz), 4.06 (dt, 1H, *J* = 9.1 Hz, 4.0 Hz), 1.82 (m, 4H), 1.50 (m, 1H), 1.41 (m, 1H), 1.34 (m, 4H), 1.23 (m, 15H), 1.16 (m, 2H), 0.89 (t, 3H, *J* = 6.3 Hz), 0.87 (t, 3H, *J* = 5.9 Hz). ^{13}C NMR (500 MHz, $CDCl_3$) δ: 166.0, 133.1, 130.0, 128.5, 75.7, 63.9, 38.7, 34.6, 32.0, 31.4, 29.6, 29.5, 29.4 29.3, 29.0, 27.9, 27.2, 26.7, 25.7, 22.7, 22.6, 22.5, 14.1. IR (neat): $\tilde{\nu}$ = 2945, 2880, 1721, 1266, 1108, 1069, 709 cm^{-1}. $[\alpha]_D^{25}$: +6.4 (c 0.68, CCl_4).

(7*R*, 8*R*)-8-Chloro-2-methyloctadecan-7-yl benzoate-d$_4$, $^{17}O_2$ (+)-6b

The compound (+)-**6** (0.00024 mol) and 20 % Pd/C. 0.093 g, 92 %, colorless oil: ^{1}H NMR (500 MHz, $CDCl_3$) δ: 8.10–8.08 (d, 2H, *J* = 7.2 Hz), 7.59–7.56 (t, 1H, *J* = 7.4 Hz), 7.48–7.45 (t, 2H, *J* = 7.7 Hz), 5.30–5.28 (m, 1H), 4.08–4.05 (dt, 1H, *J* = 9.1 Hz, 4.0 Hz), 1.83–1.69 (m, 3H), 1.53–148 (m, 1H), 1.33–1.24 (m, 19H), 0.87 (t, 3H, *J* = 6.3 Hz), 0.84 (d, 6H, *J* = 6.6 Hz). ^{13}C NMR (500 MHz, $CDCl_3$) δ: 165.9, 165.8 ($^{13}C_{benzoate}$-^{17}O), 133.0, 129.9, 129.7, 129.6, 128.3, 75.5, 75.4 ($^{13}C_{benzoate}$-^{17}O), 63.7, 38.6, 34.4, 31.8, 29.5, 29.4, 29.3, 29.2 28.9, 27.7, 26.5, 22.6, 22.5, 22.4, 14.0. IR (neat): $\tilde{\nu}$ = 2945, 2880, 1721, 1266, 1108, 1069, 709 cm^{-1}. $[\alpha]_D^{25}$: +6.4 (c 0.68, CCl_4).

(7*R*, 8*R*)-8-Chloro-2-methyloctadecan-7-yl benzoate-d$_4$, $^{18}O_2$ (+)-6c

The compound (+)-**6** (0.00024 mol) and 20 % Pd/C. 0.093 g, 92 %, colorless oil: ^{1}H NMR (500 MHz, $CDCl_3$) δ: 8.09–8.08 (d, 2H, *J* = 7.2 Hz), 7.59–7.56 (t, 1H, *J* = 7.4 Hz), 7.48–7.45 (t, 2H, *J* = 7.7 Hz), 5.29–5.27 (m, 1H), 4.07–4.04 (dt, 1H, *J* = 9.1 Hz, 4.0 Hz), 1.81–1.69 (m, 2H), 1.53–1.47 (m, 1H), 1.30–1.23 (m, 20H), 0.87 (t, 3H, *J* = 6.3 Hz), 0.85 (d, 6H, *J* = 6.6 Hz). ^{13}C NMR (500 MHz, $CDCl_3$) δ: 165.9, 165.8 ($^{13}C_{benzoate}$-^{18}O), 133.0, 129.9, 129.7, 128.3, 75.5, 75.4 ($^{13}C_{benzoate}$-^{18}O), 63.7, 38.6, 34.4, 31.8, 29.5, 29.4, 29.3 29.2, 28.9, 27.8, 26.5, 22.6, 22.5, 22.4, 14.0. IR (neat): $\tilde{\nu}$ = 2955, 2888, 1727, 1266, 1110, 1080, 709 cm^{-1}. HRMS (ESI) *m/z* calculated for $C_{26}H_{39}ClKD_4{}^{18}O_2$ [M + K]: 467.2888, found 467.2876. $[\alpha]_D^{25}$: +6.4 (c 0.68, CCl_4).

(7*S*, 8*S*)-8-Chloro-2-methyloctadecan-7-yl benzoate (–)-6

Yield 1.10 g, 90 %, colorless oil: ^{1}H NMR (500 MHz, $CDCl_3$) δ: 8.09–8.08 (d, 2H, *J* = 7.2 Hz), 7.57 (t, 1H, *J* = 7.4 Hz), 7.48–7.45 (t, 2H, *J* = 7.7 Hz), 5.31–5.28 (dt, 1H, *J* = 7.2 Hz, 3.2 Hz), 4.08–4.04 (dt, 1H, *J* = 9.1 Hz, 4.0 Hz), 1.88–1.80 (m, 4H), 1.69–1.53 (m, 1H), 1.41 (m, 1H), 1.34 (m, 4H), 1.24 (m, 15H), 0.89 (t, 3H, *J* = 6.3 Hz), 0.85 (d, 6H, *J* = 6.6 Hz). ^{13}C NMR (500 MHz, $CDCl_3$) δ: 165.9, 133.0, 130.0, 129.7, 128.3, 75.6, 63.7, 38.7, 34.4, 31.8, 31.3, 29.6, 29.5, 29.4 29.3, 29.2, 29.0, 27.8, 27.1, 26.5, 25.5, 22.6, 22.5, 22.4, 14.0. IR (neat): $\tilde{\nu}$ = 2945, 2880, 1721, 1266, 1108, 1069, 709 cm^{-1}. HRMS (ESI) *m/z* calculated for $C_{26}H_{43}ClO_2$ [M + H]: 424.0792, found 424.2289. $[\alpha]_D^{25}$: –6.35 (c 0.68, CCl_4).

(7*S*, 8*S*)-8-Chloro-2-methyloctadecan-7-yl benzoate-d$_4$, $^{17}O_2$ (–)-6b

The compound (–)-**6** (0.00024 mol) and 20 % Pd/C. 0.093 g, 92 %, colorless oil: ^{1}H NMR (500 MHz, $CDCl_3$) δ: 8.09–8.08 (d, 2H, *J* = 7.2 Hz), 7.60–7.56(t, 1H, *J* = 7.4 Hz), 7.48–7.44 (t, 2H, *J* = 7.7 Hz), 5.31–5.27 (m, 1H), 4.08–4.04 (dt, 1H, *J* = 9.1 Hz, 4.0 Hz), 1.87–1.71 (m, 3H), 1.54–147 (m, 1H), 1.34–1.23 (m, 19H), 0.87 (t, 3H, *J* = 6.3 Hz), 0.84 (d, 6H, *J* = 6.6 Hz). ^{13}C NMR (500 MHz, $CDCl_3$) δ: 165.9, 165.8 ($^{13}C_{benzoate}$-^{17}O), 133.0, 129.9, 129.7, 129.6, 128.3, 75.5, 75.4 ($^{13}C_{benzoate}$-^{17}O), 63.7, 38.6, 34.4, 31.8, 29.5, 29.4, 29.3, 29.2 28.9, 27.7, 26.5, 22.6, 22.5, 22.4, 14.0. IR (neat): $\tilde{\nu}$ = 2945, 2880, 1721, 1266, 1108, 1069, 709 cm^{-1}. $[\alpha]_D^{25}$: –6.37 (c 0.68, CCl_4).

(7*S*, 8*S*)-8-Chloro-2-methyloctadecan-7-yl benzoate-d$_4$, $^{18}O_2$ (–)-6c

The compound (–)-**6** (0.00024 mol) and 20 % Pd/C. 0.093 g, 92 %, colorless oil: ^{1}H NMR (500 MHz, $CDCl_3$) δ: 8.10–8.08 (d, 2H, *J* = 7.2 Hz), 7.60–7.56 (t, 1H, *J* = 7.4 Hz), 7.48–7.45 (t, 2H, *J* = 7.7 Hz), 5.31–5.28 (m, 1H), 4.08–4.04 (dt, 1H, *J* = 9.1 Hz, 4.0 Hz), 1.83–1.71 (m, 2H), 1.53–1.47 (m, 1H), 1.30–1.23 (m, 20H), 0.87 (t, 3H, *J* = 6.3 Hz), 0.85 (d, 6H, *J* = 6.6 Hz). ^{13}C NMR (500 MHz, $CDCl_3$) δ: 165.9, 165.8 ($^{13}C_{benzoate}$-^{18}O), 133.0, 129.9, 129.7, 128.3, 75.5, 75.4 ($^{13}C_{benzoate}$-^{18}O), 63.7, 38.6, 34.4, 31.8, 29.5, 29.4, 29.3 29.2, 28.9, 27.8, 26.5, 22.6, 22.5, 22.4, 14.0. IR (neat): $\tilde{\nu}$ = 2955, 2888, 1727, 1266, 1110, 1080, 709 cm^{-1}. HRMS (ESI) *m/z* calculated for $C_{26}H_{39}ClKD_4{}^{18}O_2$ [M + K]: 467.2888, found 467.2876. $[\alpha]_D^{25}$: –6.4 (c 0.68, CCl_4).

General procedure for Preparation of (+)-1, (+)-1a, (+)-1b, (+)-1c, (–)-1, (–)-1b and (–)-1c

To an ice cold, stirred solution of (+)-**6** or (–)-**6** (0.9456 mmol) in methanol (6 mL), 4 N NaOH in methanol (4 mL) was added slowly to the reaction flask. The resulting mixture was stirred at room temperature for 2 h. The reaction solvent was removed by evaporation under reduced pressure and diluted with ethyl acetate (20 mL) and water (10 mL). The phases were separated, and the aqueous phase was extracted with ethyl acetate (3 × 20 mL). The combined organic layers were washed with brine (10 mL), dried with $MgSO_4$, and concentrated under reduced pressure. Purification of the crude product by flash chromatography (silica gel, 100 % hexanes) afforded (+)-disparlure or (–)-disparlure.

(7*R*, 8*S*)-7, 8-Epoxy-2-methyloctadecane (+)-1

(Eluent: 100 % hexane), 0.240 g, 90 %, clear oil: ^{1}H NMR (500 MHz, $CDCl_3$) δ: 2.92–2.88 (m, 2H), 1.56–1.18 (m, 27H), 0.90–0.85 (m, 9H). ^{13}C NMR (500 MHz, $CDCl_3$) δ: 57.4, 39.0, 32.0, 29.7, 29.7, 28.0, 27.9, 27.0, 26.7, 22.8, 22.7, 22.7, and 14.2. IR (neat): $\tilde{\nu}$ = 2954, 2923, 2854, 1466, 1385, 1029, 721 cm^{-1}. HRMS (ESI) *m/z* calculated for $C_{19}H_{38}O$ [M + H]: 283.3001, found 283.2985. $[\alpha]_D^{25}$: +0.54 (c 0.56, CCl_4).

(7*R*, 8*S*)-7, 8-Epoxy-2-octadecane (+)-1a

(Eluent: 100 % hexane), 0.242 g, 91 %, clear oil: ^{1}H NMR (500 MHz, $CDCl_3$) δ: 2.92–2.88 (m, 2H), 1.56–1.18 (m, 27H), 0.90–0.85 (m, 6H). ^{13}C NMR (500 MHz, $CDCl_3$) δ: 57.4, 39.0, 32.0, 29.7, 29.7, 28.0, 27.9, 27.0, 26.7, 22.8, 22.7, 22.7, and 14.2. IR (neat): $\tilde{\nu}$ = 2954, 2923, 2854, 1466, 1385, 1029, 721 cm^{-1}. $[\alpha]_D^{25}$: +0.55 (c 0.56, CCl_4).

(7*R*, 8*S*)-7, 8-Epoxy-2-methyloctadecane-d$_4$,^{17}O (+)-1b

The compound (+)-**6** (0.000163 mol) and 4 N NaOH. (Eluent: 100 % hexane), 0.042 g, 90 %, clear oil: ^{1}H NMR (500 MHz, $CDCl_3$) δ: 2.92–2.88 (m, 2H), 1.56–1.16 (m, 23H), 0.89–0.86 (m, 9H). ^{13}C NMR (500 MHz, $CDCl_3$) δ: 57.2–57.0 ($^{13}C_{epo}$-^{2}H & $^{13}C_{epo}$-^{17}O), 38.8, 31.8, 29.5, 29.4, 29.2, 27.8, 27.7, 26.5, 22.6, 22.6, 22.5, and 14.0. IR (neat): $\tilde{\nu}$ = 2954, 2923, 2854, 1466, 1385, 1029, 721 cm^{-1}. HRMS (ESI) *m/z* calculated for $C_{19}H_{35}D_4{}^{17}O$ [M + H]: 288.3281, found 288.3288. $[\alpha]_D^{25}$: +0.54 (c 0.56, CCl_4).

(7*R*, 8*S*)-7, 8-Epoxy-2-methyloctadecane-d$_4$,^{18}O (+)-1c

The compound (+)-**6** (0.000163 mol) and 4 N NaOH. (Eluent: 100 % hexane), 0.042 g, 89.5 %, clear oil: ^{1}H NMR (500 MHz, $CDCl_3$) δ: 2.92–2.89 (m, 2H), 1.56–1.18 (m, 23H), 0.90–0.85 (m, 9H). ^{13}C NMR (500 MHz, $CDCl_3$) δ: 57.2–57.0 ($^{13}C_{epo}$-^{2}H & $^{13}C_{epo}$-^{18}O), 39.0, 32.0, 29.7, 29.5, 29.4, 29.2, 27.8, 27.7, 26.5, 22.6, 22.5, 22.4, and 14.0. IR (neat): $\tilde{\nu}$ = 2954, 2923, 2854, 1466, 1385, 1029, 721 cm^{-1}. HRMS (ESI) *m/z* calculated for $C_{19}H_{34}D_4Na{}^{18}O$ [M + Na]: 311.3120, found 311.3108. $[\alpha]_D^{25}$: +0.54 (c 0.56, CCl_4).

(7*S*, 8*R*)-7, 8-Epoxy-2-methyloctadecane (–)-1

(Eluent: 100 % hexane), 0.240 g, 90 %, clear oil: ^{1}H NMR (500 MHz, $CDCl_3$) δ: 2.91–2.87 (m, 2H), 1.53–1.19 (m, 27H), 0.89–0.86 (m, 9H).

^{13}C NMR (500 MHz, $CDCl_3$) δ: 57.2, 57.0, 38.8, 31.8, 29.7, 29.1, 27.9, 27.8, 27.7, 27.6, 27.2, 26.7, 26.4, 22.6, 22.5, 22.5, 22.4, 14.2, 14.01. IR (neat): $\tilde{\nu}$ = 2954, 2923, 2854, 1466, 1385, 1029, 721 cm^{-1}. HRMS (ESI) *m/z* calculated for $C_{19}H_{38}O$ [M + H]: 283.3001, found 283.2985. $[\alpha]_D^{25}$: –0.537 (c 0.56, CCl_4).

(7*S*, 8*R*)-7, 8-Epoxy-2-methyloctadecane- d_4,^{17}O (–)-1b

The compound (–)-**6** (0.000163 mol) and 4 N NaOH. (Eluent: 100 % hexane), 0.039 mg, 83 %, clear oil: ^1H NMR (500 MHz, $CDCl_3$) δ: 2.92–2.89 (m, 2H), 1.56–1.16 (m, 23H), 0.89–0.86 (m, 9H). ^{13}C NMR (500 MHz, $CDCl_3$) δ: 57.2–57.0 ($^{13}C_{epo}$-^2H & $^{13}C_{epo}$-^{17}O), 38.8, 31.8, 29.5, 29.4, 29.2, 27.8, 27.7, 26.5, 22.6, 22.6, 22.5, and 14.0. IR (neat): $\tilde{\nu}$ = 2954, 2923, 2854, 1466, 1385, 1029, 721 cm^{-1}. HRMS (ESI) *m/z* calculated for $C_{19}H_{35}D_4{}^{17}O$ [M + H]: 288.3281, found 288.3288. $[\alpha]_D^{25}$: –0.535 (c 0.56, CCl_4).

(7*S*, 8*R*)-7, 8-Epoxy-2-methyloctadecane d_4,^{18}O (–)-1c

The compound (–)-**6** (0.000163 mol) and 4 N NaOH. (Eluent: 100 % hexane), 0.041 g, 87 %, clear oil: ^1H NMR (500 MHz, $CDCl_3$) δ: 2.92–2.89 (m, 2H), 1.56–1.18 (m, 23H), 0.90–0.85 (m, 9H). ^{13}C NMR (500 MHz, $CDCl_3$) δ: 57.2–57.0 ($^{13}C_{epo}$-^2H & $^{13}C_{epo}$-^{18}O), 39.0, 32.0, 29.7, 29.5, 29.4, 29.2, 27.8, 27.7, 26.5, 22.6, 22.5, 22.4, and 14.0. IR (neat): $\tilde{\nu}$ = 2954, 2923, 2854, 1466, 1385, 1029, 721 cm^{-1}. HRMS (ESI) *m/z* calculated for $C_{19}H_{34}D_4Na^{18}O$ [M + Na]: 311.3120, found 311.3108. $[\alpha]_D^{25}$: –0.535 (c 0.56, CCl_4).

Acknowledgments

This research was supported by Discovery grants from the Natural Sciences and Engineering Research Council (NSERC) of Canada # 22923-2010 and 2015-06088, as well as by Discovery Accelerator Supplement # 477793-2015. We thank Ms. Nathalie Leva (USDA) for assistance with the field trial in Massachusetts.

Keywords: Gypsy moth · Disparlure enantiomers · LdisPBPs · Isotope labelling · Mitsunobu inversion

[1] B. A. Bierl, M. Beroza, C. W. Collier, *Science* **1970**, *170*, 87–89.
[2] S. Iwaki, S. Marumo, T. Satio, M. Yamada, K. Katagiri, *J. Am. Chem. Soc.* **1974**, *96*, 7842–7844.
[3] E. Plettner, J. Lazar, E. G. Prestwich, G. D. Prestwich, *Biochemistry* **2000**, *39*, 8953–8962.
[4] Y. Gong, T. C. S. Pace, C. Castillo, C. Bohne, M. A. O'Neill, E. Plettner, *Chem. Biol.* **2009**, *16*, 162–172.
[5] Y. Yu, E. Plettner, *Bioorg. Med. Chem.* **2013**, *21*, 1811–1822.
[6] J. T. Sanes, E. Plettner, *Arch. Biochem. Biophys.* **2016**, *606*, 53–63.
[7] For synthesis of (+)-disparlure over last two decades, see: a) E. Fukusaki, S. Senda, Y. Nakazono, H. Yuasa, T. Omata, *J. Ferment. Bioeng.* **1992**, *73*, 284–286; b) J. L. Brevet, K. Mori, *Synthesis* **1992**, 1007–1012; c) S. Tsuboi, H. Furutani, M. H. Ansari, T. Sakai, M. Utaka, A. Takeda, *J. Org. Chem.* **1993**, *58*, 486–492; d) S. Y. Ko, *Tetrahedron Lett.* **1994**, *35*, 3601–3604; e) A. Sinha-Bagchi, S. C. Sinha, E. Keinan, *Tetrahedron: Asymmetry* **1995**, *6*, 2889–2892; f) J. A. Marshall, J. A. Jablonowski, H. J. Jiang, *J. Org. Chem.* **1999**, *64*, 2152–2154; g) A. E. Koumbis, D. D. Chronopoulos, *Tetrahedron Lett.* **2005**, *46*, 4353–4355; h) C. X. Zhang, S. J. Da, H. B. Zhang, B. Sun, Y. Li, *Acta Chim. Sinica* **2007**, *65*, 2433–2436; i) K. R. Prasad, P. Anbarasan, *Russ. J. Org. Chem.* **2007**, *72*, 3155–3157; j) V. N. Kovalenko et al., *Russ. J. Org. Chem.* **2009**, *45*, 1318–1324; k) A. K. Dudey, A. Chattopadhyay, *Tetrahedron: Asymmetry* **2011**, *22*, 1516–1521; l) W. Zhigang, Z. Jianfeng, H. Peiqiang, *Chin. J. Chem.* **2012**, *30*, 23–28; m) V. Bethi, P. Kattanguru, R. A. Fernandes, *Eur. J. Org. Chem.* **2014**, 3249–3255.
[8] a) L. H. Li, D. Wang, T. H. Chan, *Tetrahedron Lett.* **1981**, *103*, 464–466.
[9] E. Keinan, S. C. Sinha, A. Sinhabagchi, Z. M. Wang, X. L. Zhang, K. B. Sharpless, *Tetrahedron Lett.* **1992**, *33*, 6411–6414.
[10] See ref.[7f].
[11] T. Sato, T. Itoh, T. Fujisawa, *Tetrahedron Lett.* **1987**, *28*, 5677–5680.
[12] a) S. J. Hu, S. Jayaraman, A. C. Oehlschlager, *J. Org. Chem.* **1999**, *64*, 3719–3721; b) Y. Garg, A. K. Tiwari, S. K. Pandey, *Tetrahedron Lett.* **2017**, *58*, 3344–3346.
[13] See ref.[2].
[14] a) K. Mori, T. Takigawa, M. Matsui, *Tetrahedron* **1979**, *35*, 833–837; b) K. R. Prasad, P. Anbarasan, *J. Org. Chem.* **2007**, *72*, 3155–3157.
[15] F. Grater, W. Xu, W. Leal, H. Grubmuller, *Structure* **2006**, *14*, 1577–1586.
[16] R. Maida, A. Steinbrecht, G. Ziegelberger, P. Pelosi, *Insect Biochem. Mol. Biol.* **1993**, *23*, 243–253.
[17] J. Krieger, H. Breer, *Science* **1999**, *286*, 720–723.
[18] Y. Gong, H. Tang, C. Bohne, E. Plettner, *Biochemistry* **2010**, *49*, 793–801.
[19] R. G. Vogt, A. C. Kohne, J. T. Dubnau, G. D. Prestwich, *J. Neurosci.* **1989**, *9*, 3332–3346.
[20] M. P. Brochu, S. P. Brown, D. W. C. MacMillan, *J. Am. Chem. Soc.* **2004**, *126*, 4108–4109.
[21] M. Amatore, T. D. Beeson, S. P. Brown, D. W. C. MacMillan, *Angew. Chem. Int. Ed.* **2009**, *48*, 5121–5124; *Angew. Chem.* **2009**, *121*, 5223.
[22] D. Bernard, A. Doutheau, J. Gore, J. Moulinoux, V. Quemener, J. Chantepie, G. Quash, *Tetrahedron* **1989**, *45*, 1429–1439.
[23] H. Brinkmann, R. W. Hoffmann, *Chemische Ber.* **1990**, *123*, 2395–2401.
[24] J. W. Concellon, H. Rodriguez-Solla, C. Simal, C. Gomez, *Synlett* **2007**, 75–78.
[25] B. Kang, R. Britton, *Org. Lett.* **2007**, *9*, 5083–5086.
[26] D. G. Ott, In *Synthesis with stable isotopes of carbon, nitrogen and oxygen*, John & Wiley Sons, New York, **1981**.
[27] G. W. Kabalaka, N. M. Goudgaon, *^{17}O-enriched methods*. In *^{17}O NMR spectroscopy in organic chemistry*, CRC Press, Boca Raton, Flo, **1991**, p. 21–37.
[28] M. W. Skidmore, *Handbook of Derivatives for Chromatography*, 2nd ed. John Wiley & Sons, **1993**.
[29] J. E. Oliver, R. M. Waters, *J. Chem. Ecol.* **1995**, *2*, 199–211.
[30] J. Nardella, M. Terrado, N. Honson, E. Plettner, *Arch. Biochem. Biophys.* **2015**, *579*, 73–84.
[31] K. Tori, K. Aono, K. Kitahonoki, R. Muneyuki, Y. Takano, H. Tanida, T. Tsuji, *Tetrahedron Lett.* **1966**, *25*, 2921–2926.
[32] C. R. Cantor, P. R. Schimmel, *Biophysical Chemistry, Part II: Techniques for the study of biological structure and function*. (Freeman, W. H & Co. **1980**).
[33] M. Terrado, Y. Yu, E. Plettner, *Can. J. Chem.* **2018**, *96*, 168–177.
[34] D. Schneider, W. A. Kafka, M. Beroza, B. A. Bierl, *J. Comp. Physiol.* **1977**, *113*, 1–15.
[35] R. L. Vold, J. S. Waugh, M. P. Kelvin, D. E. Phelps, *J. Chem. Phys.* **1968**, *48*, 3831–3832.
[36] S. Meiboom, D. Gill, *Rev. Sci. Instrum.* **1958**, *29*, 688–691.
[37] M. Biasini, S. Bertoni, A. Waterhouse, K. Arnold, G. Studer, T. Schmidt, F. Kiefer, T. G. Cassarino, M. Bertoni, L. Bordoli, T. Schwede, *Nucleic Acids Res.* **2014**, *42*, 252–258.
[38] T. J. S. Merritt, S. Laforest, G. D. Prestwich, J. M. Quattro, R. G. Vogt, *J. Mol. Evol.* **1998**, *46*, 272–276.
[39] Chemical Computing Group, Molecular Operating Environment, Canada, Quebec city, C **2011**.
[40] E. Kleinpeter, S. Kruger, A. Koch, *J. Phys. Chem. A* **2015**, *119*, 4268–4276.
[41] Plimmer et al., *Environ. Entomol.* **1977**, *6*, 518–522.

Received: August 6, 2019

Enantioselective Recognition

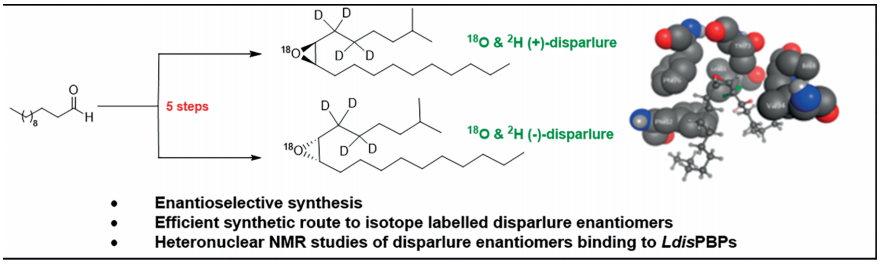

Disparlure, (7R, 8S)-epoxy-2-methyloxtadecane, is the sex pheromone of the gypsy moth. Its shortest synthesis, in high (> 99 %) enantiomeric excess is reported. Furthermore, the incorporation of stable isotope labels into disparlure and studies by ^{2}H NMR of the interaction between disparlure enantiomers and the two pheromone-binding proteins found in the antennae of male gypsy moths in described.

DOI: 10.1002/ejoc.201901164